R. & M. No. 3640

R. & M. No. 3640



MINISTRY OF TECHNOLOGY

AERONAUTICAL RESEARCH COUNCIL
REPORTS AND MEMORANDA

# Low-Speed Wind-Tunnel Tests on a Wing-Fuselage Model with Area Suction Through Perforations at the Leading-Edge Flap Knee

By S. F. J. Butler
and
J. A. Lawford
Aerodynamics Dept., R.A.E. Farnborough

LONDON: HER MAJESTY'S STATIONERY OFFICE
1970
PRICE £1 10*s* 0*d* [£1·50] NET

# Low-Speed Wind-Tunnel Tests on a Wing-Fuselage Model with Area Suction Through Perforations at the Leading-Edge Flap Knee

By S. F. J. BUTLER
and
J. A. LAWFORD
Aerodynamics Dept., R.A.E. Farnborough

*Reports and Memoranda No.* 3640*
*July*, 1967

*Summary.*

Distributed suction may be preferable to tangential blowing as a method of boundary-layer control to achieve high lift for civil aircraft, because of its lower flow rates and power requirements. Tests using practical perforated suction surfaces at the knee of full-span L.E. flaps are reported, for conventional hinged flaps and for an extending-area arrangement having increased knee radius.

Stalling incidence increased progressively with suction rate. With T.E. flaps extended, a $C'_Q$ of 0·0024 increased $C_{L_{max}}$ from 2·17 (at $\alpha_w = 17{\cdot}5°$) to 2·68 ($\alpha_w = 28{\cdot}3°$), and from 2·47 ($\alpha_w = 25°$) to 2·80 ($\alpha_w = 33°$) for hinged and extending L.E. flaps respectively: increments with T.E. flaps retracted were similar.

Flow requirements were insensitive to perforation arrangement and were little affected by simulated heavy rain; they were significantly reduced by increase of open-area ratio (with accompanying fall of plenum chamber depression and suction power) and increased by surface imperfections and inter-surface leaks.

Extending-area L.E. flaps may have advantages even without B.L.C., if mechanically practicable.

LIST OF CONTENTS



*Replaces R.A.E. Technical Report No. 67 153—A.R.C. 29 756.

LIST OF CONTENTS—*continued*



*Section*

1. *Introduction.*

Extensive B.L.C. research investigations on military aircraft applications have been made at the Royal Aircraft Establishment, concerning the usefulness of high-pressure tangential slot blowing for high lift[1]. Particularly for civil transport applications of high-lift boundary-layer control, because flow rates and power requirements at take-off are then of paramount importance, the alternative use of distributed suction through a suitable porous surface merited consideration if technically feasible. NASA had already made successful wind-tunnel model tests[2] and prototype aircraft flight tests[3] on the F-86A with distributed suction through high-resistance felted surfaces. Therefore, in conjunction with Hawker Siddeley Aircraft (Hatfield), it was decided to develop and assess practical perforated suction surface arrangements with simple internal wing ducts, for use at the knee of deflected L.E. flaps.

A large model was considered essential to allow the use of hole sizes and spacings appropriate to full-scale conditions. Consequently the experimental difficulties and inferior airflow characteristics of the R.A.E. 24 ft open-jet wind tunnel were accepted. For most of the tests, made between 1961 and 1964*, the Reynolds number (based on wing chord) was $2{\cdot}0 \times 10^6$, with a few checks at $2{\cdot}6 \times 10^6$; this was considered adequate for the present research comparisons. The same basic wing-fuselage configuration was adopted as that employed by H.S.A. (Hatfield) for their own allied high-lift investigations at comparable Reynolds numbers on small-scale half-models. The 10 per cent thick, constant section, aspect ratio 5 untapered 31° sweptback wing was sufficiently similar to the aspect ratio 4·8, 35° sweepback

F-86A configuration for direct research comparisons to be made.

In addition to measurements of the three longitudinal components, studies were made of wing surface pressure distributions, suction inflow characteristics, wing boundary-layer development, and stalling behaviour. A comparative evaluation of different suction surfaces was made, both with a conventional hinged L.E. flap and with an extending-area L.E. flap incorporating an increased knee radius. The effects of practical surface imperfections, and of rain, were investigated.

2. *Model and Test Details.*

The model, which was constructed by H.S.A. (Hatfield), was of simple basic design (*see* Table 1, Figs. 1, 2 and 3), having a 31° sweptback A.R.5 wing (10 per cent thick section streamwise, with some nose camber) without taper, twist, or dihedral. A light-aircraft form of construction was adopted for the wing, with plywood forming most of the external surfaces. The wing was set in a low position on the cylindrical centre section of the body of revolution constituting the fuselage, which was not equipped with a fin or tailplane. The wing was provided with full-span 35 per cent chord T.E. Fowler flaps (*see* Figs. 1, 2 and 6), which were either fully retracted or else extended and set at 35° deflection streamwise (corresponding to a deflection of 40° normal to hinge-line). Two types of L.E. flap were considered, the wing and flap profile being maintained continuous to the fuselage surface. The conventional L.E. flap, with settings of 32° and 37° streamwise (36° and 41° respectively normal to L.E.), had a hinge-line just inside the wing lower surface at 13 per cent chord (*see* Fig. 4). The extending-area L.E. flap, with settings of 31° and 36° streamwise (35° and 40° respectively normal to L.E.), was designed to provide a 3·4 per cent chordwise extension when retracted, together with further extensions of 5·55 per cent and 5·72 per cent of the increased basic chord on deflection to 31° and 36° respectively (*see* Fig. 5). Each L.E. flap had the same slightly cambered nose section with a L.E. radius of about 0·75 per cent chord streamwise (about 1 per cent normal to L.E.). The radius of the knee of the conventional L.E. flap was about 7·5 per cent chord (in the plane normal to the L.E.), the radius of the knee of the extending-area L.E. flap being some 2·5 times larger, about 18·5 per cent chord (in the plane normal to the L.E.).

The model scale was made as large as feasible, bearing in mind tunnel constraint considerations, to facilitate the construction of practical suction surfaces and allow tests of full-scale perforations. Each L.E. flap was fitted with a plenum chamber, divided into seven sections across the span of each wing (Fig. 3) and located below the circular-arc portion of the flap knee, with alternative perforated surface specimens providing variation of hole size and open area ratio (*see* Fig. 7). A datum perforated configuration was provided by specimen *F*, with a large number (114 holes per square inch) of small holes (0·014 inch diameter) arranged in 13 spanwise rows, giving a comparatively small open-area ratio of 1·75 per cent to ensure high surface resistance and a nearly uniform inflow distribution. The other specimens allowed comparative evaluation of more practical arrangements, including large hole sizes (up to 0·047 inch diameter), smaller numbers of holes (as few as 10 per square inch), and fewer rows (down to 4). Larger open-area ratios (up to 5·3 per cent) were also considered, with reduced resistivity and lower suction power requirements.

A rolled and sintered woven wire element was also included, which was intended to represent the idealised uniformly permeable surface of high resistivity considered in theoretical treatments. Unfortunately, the specimen proved unsuitable for this purpose, as it exhibited large local variations in resistance, together with a tendency to become contaminated in a non-uniform fashion.

In each wing, the seven suction chambers were individually connected to main collector ducts by pre-set trimming valves (*see* Fig. 3 and Section 3.2). The main wing ducts led to the fuselage ducts, which incorporated ring pitot and static tubes upstream of the suction air connector.

Usually, the model was rigged in an inverted attitude off the main struts of the 24ft tunnel three-component overhead balance, with cross-bracing by slender elliptic struts. The usual tailwire arrangement had to be modified to allow an increased net incidence range of about 30° by the use of a special, deep oil-pot (*see* Fig. 1). Also, to avoid small pitching oscillations, the counterbalance weight was finally

*The test results were analysed at the time and received a limited circulation in the form of H.S.A. (Hatfield) internal reports.

supported by an elliptic strut, rather than the wire used initially, and shown in Fig. 1.

The suction air was passed from the fuselage ducts through a special suction air connector into the vertical standpipe (*see* Fig. 8) and thence to the suction pump, *via* an orifice plate. The presence of the standpipe necessitated an opening in the aerodynamic upper surface of the fuselage (Fig. 1), and suitable sealing precautions were taken to avoid net flows through the fuselage cavity thus formed. The air-bearing connector comprised two opposed circular annulus bearings mounted on the model pitch-axis, the earth-side bearings being supported by the top section of the standpipe (Fig. 8). Auxiliary compressed air supplies were arranged to the bearing interfaces. Also, to allow for some degree of maladjustment, in lateral position and in roll, extra flexibility was provided by mounting the top section off the main standpipe by metal spring strips, with a suitable flexible seal. With adjustment of the bracing wires, this arrangement worked well and balance zeros were unaffected by the internal duct pressure. No particular problems were encountered in the presence of wind load.

During the final tests with rain simulation, for which balance measurements were not necessary and an upright model arrangment was essential, the model was supported on the struts of the lower balance, with the fuselage modified to allow the strut to enter the lower fuselage (*see* Fig. 9a). An existing rain-spray gun developed by Mechanical Engineering Department, R.A.E., was rigged ahead of the model to provide a water spray coverage over the central test section of the starboard wing (*see* Section 3.5).

Although most tests were made with a smooth wing upper surface, some of the tests on the extending-area L.E. flaps were made in the presence of vortex generators. The two types considered are shown in Figs. 10a and b; in each case, a single row extending across the full span was employed. Also, tests were made with both types of L.E. flap to investigate the sensitivity of required suction quantities to possible surface imperfections. As indicated in Fig. 10c, these included not only surface discontinuities but also simulated leaks through the wing surface.

In addition to a main chordwise static-pressure traverse at 65·6 per cent semi-span on the starboard wing (Figs. 4, 5, 6), the model instrumentation included static-pressure traverses across the knee of the L.E. flap at 3 other stations on the starboard wing and 2 stations on the port wing (*see* Fig. 3). The flap knee static tubes necessarily were attached to the insides of the various specimen surfaces and were connected by flexible tubing to hypodermic tubes passing through the wall of the plenum chamber to the main wing tube runs. The duct instrumentation comprised static-pressure tappings in each chamber and each outlet pipe (upstream of the trimming valve), together with the ring pitot and static tubes monitoring the total flow from each wing. The various pressure tubes were collected in the fuselage cavity and led down the stand-pipe, with suitable slack to minimise balance constraints; the external static-pressure tubes were temporarily disconnected for balance runs when considered necessary.

The transition position on the wing was left free, but transition was fixed by a wire on the nose of the fuselage. Most of the tests were made at a wind speed of 100 ft/s (R.N. based on $\bar{c} = 2 \times 10^6$), to avoid excessive load fluctuations on the tunnel fan blades (due to the downwash behind a large model at very high lift) and to increase the maximum available suction flow coefficient. Some check tests were made at 130 ft/s (R.N. $= 2{\cdot}6 \times 10^6$).

## 3. *Test Procedure.*

### 3.1. *Corrections.*

As noted previously, the reference wing area (with flaps retracted) was increased by some 3·4 per cent for the extending-area L.E. flap arrangement. In the reduction of the results for this configuration, due allowance has been made for these increases in wing area and mean chord, $\bar{c}$. Pitching moments have been based on $\bar{c}$ throughout and referred to the test *cg* at 0·295 $\bar{c}$ (conventional L.E. flaps) and 0·318 $\bar{c}$ (extending-area L.E. flaps). The test *cg* was displaced 1·3 per cent $\bar{c}$ off wing chord plane (towards the aerodynamic lower surface).

Allowance has been made for the effects of solid blockage and tunnel mean pitch. Further corrections have been applied to allow for the measured tares of the model support struts, bracing struts, tailwires, pre-set trimming valves (*see* Fig. 3 and Section 3.2). The main wing ducts led to the fuselage ducts, which incorporated ring pitot and static tubes upstream of the suction air connector.

Usually, the model was rigged in an inverted attitude off the main struts of the 24 ft tunnel three-

etc., and for the aerodynamic interference effects caused by the presence of the suction stand-pipe and fuselage cavity, amounting in all to $\Delta C_{L_{Rig}} = +0{\cdot}032$, $\Delta C_{D_{Rig}} = -0{\cdot}057$, and $\Delta C_{m_{Rig}} = +0{\cdot}040$ (the latter correction being mainly due to the presence of the suction strut).

Conventional open-jet tunnel constraint corrections[4] have been applied as follows:

$$\Delta\alpha \underset{\text{(degrees)}}{\text{Constraint}} = \begin{matrix} -0{\cdot}815\, C_L \text{ (conventional L.E. flaps),} \\ -0{\cdot}842\, C_L \text{ (extending-area L.E. flaps);} \end{matrix}$$

$$\Delta C_{D_{\text{Constraint}}} = -0{\cdot}0142\, C_L^2,\ -0{\cdot}0147\, C_L^2\ ;$$

$$\Delta C_{L_{\text{Constraint}}} = 0{\cdot}0142\, C_L C_D,\ 0{\cdot}0147\, C_L C_D\ .$$

It could be argued[5] that a further allowance for streamline curvature is justified for a large finite-chord model; this would have slightly increased the magnitude of $\Delta\alpha$, by some 7 per cent in the present case.

No allowance has been possible for gross deflection of the tunnel jet which can arise in an open-jet tunnel[5] in the presence of a lifting system, as such effects cannot be evaluated with sufficient accuracy at present. Further, the behaviour of the finite-length unbounded jet may be greatly affected[5] by the precise nature of the tunnel environment, particularly the tunnel collector size. Such effects could alter the incidence constraint corrections which should be applied and vary the corrected lift-incidence curve slope and the induced drag factor.

It is thought that such effects are moderate for the present tunnel environment. Admittedly, the corrected lift-incidence curve slopes are somewhat larger than comparable results[6] on the same model planform at comparable Reynolds numbers in a closed-jet tunnel, and also exceed the estimates based on Ref. 7, suggesting slight over-correction. On the other hand, the present results show close agreement with the results obtained by NASA on a similar model[2].

The present test objectives were mainly comparative in nature, and tunnel constraint considerations in this instance had to be weighed against the special need for a large model. Certainly, a smaller model scale would have been desirable if the main objective had been the production of quantitative data for a specific application.

### 3.2. *Measurement and Control of Suction Inflow Distributions.*

Care was taken initially to eliminate leaks into the permanent wing and fuselage ducting system. At each change of specimen, the new element was carefully screwed and glued into position, using a suitable compound (Thiokol). Then, the total leakage inflow rate into the suction system was determined by a standard orifice plate at representative depressions, by sealing the air-bearing connector and the perforated test surfaces. The leakage flow, which typically only amounted to some 4 per cent of the total suction inflow rate, remained reasonably constant during the tests.

Each of the fourteen sections of each perforated surface was calibrated individually (wind-off), with the remainder still sealed. The plenum chamber static pressure served as a main datum, but measurements were also made of the difference between this pressure and the static pressure in the outlet pipe (upstream of the preset control valve). At a given chamber depression, the mass-flow rates into the chambers were consistent with the nominal perforated area, provided care was taken to seal off any perforations contaminated by the glueing process. In practice, it was found advisable to seal off $\frac{1}{4}$ inch wide strips at each end of each chamber, as well as one or two rows at the extreme front and rear of each element (*see* Section 4.2.4).

The preset control valves were used to trim out the variations of plenum chamber static pressure under wind-off conditions, to ensure a uniform inflow velocity across the whole perforated area. Separate overall mass flow measurements were made for each wing in turn, with the other sealed, so as to calibrate the ring pitot and static tubes in the two fuselage ducts. These were used as the primary indication of flow rate during the tests, avoiding leakages at the air bearing.

At forward speed, the total mass-flow rate for each wing was deduced from the ring pitot-static mean differential, with proper allowance for the static pressure at the measuring station. Similarly, the differ-

ential static pressure between the outlet pipe and the plenum chamber, with due allowance for static pressure, provided a measure of the inflow rates into each element.

Typical spanwise variations of plenum chamber static pressure and mass inflow rates are shown in Figs. 11 and 12 for flow attachment conditions. Although the variations of inflow were considered acceptable, the incorporation of remotely-controlled trimming valves would have been of some advantage, and would certainly be desirable for the specific optimisation purposes of an aircraft development test. Independent control of the total flow rate from each wing, on the other hand, would certainly have been preferable, particularly during assessments of $C'_{\mu_a}$.

3.3. *Specification of Suction Inflow Coefficients.*

As usual, the suction coefficient $C_Q$ was defined in terms of the mass-flow rate through the porous surface, suitably non-dimensionalised, i.e.

$$C_Q = \frac{M}{\rho_o V_o S}$$

where $S$ is the gross wing area (with flaps retracted). The suction pump available allowed values of $C_Q$ up to 0·0022 at the usual test speed of 100 ft/sec.

For analysis and correlation purposes, an average sectional coefficient is usually preferable, related to the wing area, $S'$, spanned by the porous surface,

$$C'_Q = C'_Q \frac{S}{S'} = 1{\cdot}127\, C_Q, \text{ in the present case.}$$

From the total flow rate, measurements of static-pressure differential across the surface along the chordwise extent, $l$, of the surface, and a knowledge of the resistance characteristics of the surface, the chordwise variation of average inflow speed, $v_s$, can be estimated for distributed suction through an *equivalent*, fully-permeable surface, and

$$C'_Q \simeq \int_{\tilde{x}_o}^{\tilde{x}_o+l} \frac{\rho V_s}{\rho_o V_o} \frac{d\tilde{x}}{c}$$

where $\rho$ is the local air density of the air entering the surface.

In the case of a perforated surface, of local open-area ratio $\chi$, the chordwise variation of air speed through the holes, $V_H$, is simply related to $V_s$, since

$$\frac{V_H}{V_o} \simeq \frac{1}{\chi} \cdot \frac{V_s}{V_o}.$$

With the smaller open-area ratio specimens ($\chi = 0{\cdot}0175$), values of $\frac{V_H}{V_o}$ as high as 3·0 were applied.

3.4. *The Experimental Determination of $C'_{Q_a}$.*

As described later (Section 4.2.1), for all the model tests described herein, the model stalled as the result of separations commencing near the mid-semispan of each wing, rather than at the wing root or tip. The onset of stall could be detected in various alternative ways; by wing tufts, changes in overall forces, upper-surface pressure distributions, or plenum chamber static pressures.

In practice, it was generally most convenient to use the wing static pressures and the chamber pressures to indicate the onset or suppression of wing flow separations, and the degree of flow attachment across

the span. Usually, the wing incidence was preset at at maximum suction with fully attached flow and then the inflow rate was reduced progressively to zero and back to the maximum value. In this way, the critical inflow rates for each wing could be determined, including hysteresis effects (by comparing increasing *versus* decreasing critical flow rates). Sufficient repeats were made to confirm the general reliability of this procedure, and detailed pressure and force measurements were made at critical wing conditions, with minimum inflow rates for attachment ($C'_{Q_a}$).

This procedure was also followed for the tests with rain simulation over part of the span, when the local plenum chamber pressures provided the only convenient means for judging the degree of attachment of the local flow, in the absence of force measurements.

3.5. *The Calibration of the Rain Gun.*

The rain gun[8] (Fig. 9) generated a rain-like distribution of droplets in the wind tunnel airstream by means of an oscillating water spray. A stream of water passed through a fine tube pointing downstream in the tunnel; the tube was oscillated in a modified form of Lessajous figure in which the velocity in each plane was approximately constant, with rapid reversal at the edges. This gave a more uniform distribution of rain than a true Lessajous motion in which excessive local intensity would result from the reduced velocity of tube movement at the edges. The rain gun was designed for full-scale testing and it was not possible to produce scale droplet size: complete dynamic similarity with freely-falling rain is in any case not possible and it was decided that the correct representation of water concentration would give closest simulation of the conditions as regards the effects on the critical suction coefficient.

The coverage of water spray given by the rain gun in the 24 ft tunnel was sufficient to span completely one chamber of the suction ducting. The gun output was therefore calibrated over span and height ranges of 1·75 ft and 1·0 ft respectively, sufficient to include the test chamber (at mid-semispan on the starboard wing) and parts of the adjacent chambers. Readings were taken at nine points on a rectangular grid in the calibration plane, consisting of water concentration (by measurement of the volume of water entering an orifice normal to the stream in a given time), and droplet size (by means of a foil recorder).

Three combinations of flow rate and nozzle size which were found to give concentrations approximating to light, moderate and very heavy rain[9] were used for the rain effect tests, and calibrations were obtained as follows for these three settings.

| | Light rain | Moderate rain | Very heavy rain |
|---|---|---|---|
| Mean concentration, gm/m$^3$ | 0·14 | 0·21 | 1·4 |
| Maximum droplet diameter, mm | 1·4 | 2·2 | 2·0 |

Concentration varied from the mean by $\pm 20$ per cent approximately over the calibration grid, and droplet sizes were greater than natural mean values, which would be 0·45 mm, 1·0 mm, and 1·8 mm respectively for the three intensities[9]. However, this is considered a reasonable approximation to light, moderate, and very heavy rain conditions for the purpose of the present tests.

4. *Test Results.*

4.1. *Preliminary Tests and Scope of Main Tests.*

To allow a straightforward account, some of the early test results* with the conventional L.E. flaps are not considered in detail. In particular, some preliminary runs were made with small discontinuities between the deflected L.E. flaps and the fuselage. Tuft studies showed that the stall, which started near the middle of each wing in the absence of B.L.C., commenced at the wing root with suction applied to the L.E. flap knee. However, with the L.E. flaps extended to the fuselage, the model invariably stalled as the result of the spread of separations originating near the middle of each wing, rather than the wing root or tip. All the tests described in this Report were made with the discontinuities faired, to ensure that meaningful aerodynamic comparisons were obtained.

In addition to tests with various perforated specimen surfaces, the preliminary tests included an

appraisal of the sintered and rolled woven-wire element simulating an idealised uniformly-permeable surface. Unfortunately, although this specimen certainly delayed the onset of wing stall, the inflow requirements were rather high because of large local variations in the surface resistance, aggravated by a pronounced tendency for non-uniform contamination. A more reliable and preferable datum was provided by specimen F (*see* Fig. 7), with a large number of small, 0·014 inch diameter holes (114 holes per square inch) arranged in 13 rows, the comparatively-small open area ratio of 1·75 per cent ensuring a high surface resistance and a quasi-uniform inflow distribution.

The main tests with this and other perforated surfaces, in conjunction with the conventional (non-extending) full-span L.E. flaps, are described in Section 4.2. The results comprise force and moment measurements, wing surface pressure distributions, upper surface boundary-layer profiles, and summary graphs showing the factors affecting $C'_{Q_a}$ and suction power requirements. Comparable results for the extending-area full-span L.E. flaps are discussed in Section 4.3.

The L.E. flaps were deflected for all tests, two angular settings being available in each case. The full-span T.E. Fowler flaps were either fully retracted or else extended and deflected 35° streamwise. Throughout these main tests, the wing surface near the L.E. flap knee was smooth, without leaks.

Particularly with the extending-area L.E. flaps, the application of knee suction tended to cause the initial point of wing flow separation to move rearwards from the flap knee towards the T.E. of the main wing. Some tests were therefore made to investigate the effect of adding a row of vortex generators on the main wing behind the L.E. flap knee (*see* Section 4.4). Investigations were also made of the effect of surface imperfections, including leaks, in the vicinity of the knee of the L.E. flap (*see* Section 4.5). Finally, some tests were made (with the model upright) to determine the sensitivity of the suction requirements to rain.

4.2. *The Effect of Distributed Suction at the Knee of Conventional (Non-extending) L.E. Flaps.*

4.2.1. *Forces and moments.* The force and moment characteristics with full-span 13 per cent chord conventional L.E. flaps (Fig. 4) are shown in Fig. 13 for $C'_Q = 0$ and $C'_Q = 0{\cdot}0025$ (the maximum rate available). Other values of $C'_Q$ produced behaviour intermediate between the two extremes shown. It will be seen that the basic wing (without B.L.C.) stalled quite suddenly, with little prior rounding of the lift-incidence curve; the stalling incidence falling from about 21° to about 18° on deflection of the full-span T.E. Fowler flaps. These results were in good general agreement with tests at comparable Reynolds numbers by H.S.A. on models having the same wing-body arrangement. The corrected lift-incidence curve slopes were, however, rather higher in the present tests, suggesting that the applied constraint corrections were possibly rather too large (*see* Section 3.1).

The application of suction to the knee of the L.E. flaps had little effect below the basic wing stall, but caused the various force and moment curves to be extended almost linearly to higher incidences. At the maximum suction rate (Fig. 13), the delay in stalling incidence was about 10°. The lift loss at the stall appeared to become more sudden in the presence of suction B.L.C., at least with the T.E. flaps deflected. Although the precise setting of the L.E. flaps was not critical, the smaller deflection of 32° streamwise (37° normal to the hinge line) generally proved slightly superior. (In Fig. 13, specimens D and E can be regarded as aerodynamically identical). With the T.E. flaps retracted, $C_{L_{max}}$ rose by 0·48 from 1·22 to 1·70 with $\delta_N = 32°$. With the T.E. flap extended and deflected 35° (in streamwise plane), the value of $C_{L_{max}}$ rose by 0·51 from 2·17 to 2·68.

Tuft studies showed that the basic character of the stall remained the same throughout, with an initial separation as desired at the mid-span of each wing. At all suction conditions the port wing stalled first. At $C'_Q = 0$, the initial flow separation occurred immediately behind the L.E. flap knee. With suction applied, however, particularly at $\delta_N = 36°$, or with the T.E. flap retracted, there was a tendency for an initial flow disturbance further aft on the wing; this disturbed region spread quickly forwards to the knee, so that extensive separation still occurred simultaneously between the L.E. flap knee and the T.E. of the wing, with an associated sudden break in the lift curve.

---

*Detailed results are available for reference on application to the Librarian, Aerodynamics Department, R.A.E.

The method generally used for determining the critical inflow rates for each wing has already been discussed (Section 3.4): the model was set at a given incidence and the effect of variation of $C'_Q$ studied, using wing static and chamber static pressure changes to indicate the onset of flow detachment. This method was preferable because changes in the chamber static pressure gave a complete and rapid indication of flow separation, and showed its spanwise spread. The alternative method of observing the associated lift variations was less satisfactory because of the need to re-balance the weighbeam in order to assess the magnitude of any change. However it was equally definitive, as can be seen in Fig. 14a, which shows typical variations of $C_L$ with $C'_Q$ at various incidences. This figure also indicates the consistent nature of the asymmetry between the two wings, equivalent to about 2° in stalling incidence. These curves were measured with decreasing values of $C'_Q$, and the critical values have been evaluated for each wing separately. It will be seen that the post-stall value of $C'_Q$ was usually slightly higher than $C'_{Q_a}$; this was the result of increased inflow on collapse of the external pressure distribution. Rather surprisingly, checks with increasing $C'_Q$ values showed only small hysteresis effect on the variation of $C_L$ with $C'_Q$ (Fig. 14b). This was not so in the NASA tests[2]. Fig. 14c indicates that the smaller sealing strips subsequently used at chamber junctions to ensure uniform and consistent inflow calibrations (*see* Section 3.2), caused no significant effects on flow requirements. Fig. 14d shows the comparative insensitivity to small variations in chordwise extent of open area (*see* Sections 4.2.4 and 4.3.4). With the conventional L.E. flap the chordwise extent of the perforated area was 3 to $3\frac{1}{2}$ per cent chord.

4.2.2. *Surface pressure distributions.* Typical variations across the span of chordwise pressure distributions at the knee of the conventional L.E. flaps are shown in Fig. 15 for various incidences. At a given incidence, the distribution at the outer traverse on the port wing ($y = 0{\cdot}466\ b/2$) is markedly different in character from that at the corresponding position on the starboard wing, with a peak further forward at the knee and slightly higher maximum values of $-C_p$. The distributions on the two wings at $y = 0{\cdot}275\ b/2$, on the other hand, were very similar. Dimensional checks on the two wings did not show significant differences; moreover, the same general type of behaviour occurred with various surface elements, with the extended leading-edge flap (*see* Section 4.3.2) and with the model upright (for the rain tests). It seems likely that this difference in behaviour was due to tunnel airflow characteristics. A recent calibration[10] of the 24 ft tunnel flow has shown a distribution of pitch which could have resulted in increased incidence and early stall for the starboard wing rather than the port. However there could be associated chordwise curvature of the flow which might alter the effective wing camber in opposite senses on the two sides; the calibration also indicated spanwise variations of pitch and side-wash which might have contributed towards differences in behaviour between the two wings.

The pressure distributions at the four spanwise stations on the starboard wing were generally satisfactory, indicating slightly more extreme values of $C_p$ at each incidence at the middle of the wing semispan, consistent with initial flow separation in this area. It is also important to note that the stall of the port wing did not noticeably affect the development of the starboard wing pressure distributions. Thus it was possible to treat the two wings separately, and to concentrate attention on the behaviour of the more fully instrumented starboard wing.

In view of Fig. 15, the extended traverses at $y = 0{\cdot}656\ b/2$ on the starboard wing (Fig. 16) are reasonably representative of the extreme conditions attained on this wing. Various cases are presented, to show the effect of T.E. flaps, L.E. flap setting, and suction. With the T.E. flaps retracted, the application of suction allowed much higher values for $-C_p$ at the L.E. flap knee, with significantly larger peaks at the leading edge and displacement of the front stagnation point round the lower surface towards the trailing edge. The effects of suction with the T.E. flaps extended and deflected were similar, with correspondingly increased peak values and more severe gradients. At both $C'_Q = 0$ and $C'_Q = 0{\cdot}0025$, a comparison at given incidence between $\delta_N = 32°$ and $\delta_N = 37°$ shows that the latter arrangement increased the peaks at the flap knee and reduced those at the leading edge, as would be expected.

With the T.E. flap retracted, the divergence[11] of the upper surface static pressure at high incidence indicated the deterioration of the boundary layer near the trailing edge, particularly at $\delta_N = 37°$ (Figs. 16a to c); nevertheless, as shown by tufts, the onset of significant separations was associated with a

full-chord flow collapse. With the T.E. flaps extended and deflected there was some indication of pressure divergence towards the rear of the main wing (Figs. 16d to g) but little or no corresponding effects on the T.E. flap (Fig. 17). Thus, as suggested by the tuft studies, the presence of the T.E. Fowler flap appeared to reduce the tendency for trailing-edge separations, even with suction applied to avoid leading-edge flow separations.

4.2.3. *Boundary layer investigations.* Because of the difficult nature of the test environment, the boundary-layer studies were limited to exploratory total-head measurements at $y = 0{\cdot}656\ b/2$ on the starboard wing, the location of the main static-pressure traverse. Pitot rakes were attached to the wing and aligned in the direction of the local surface streamline (assessed by wing tufts, taking a mean value over the incidence range). Four chordwise stations were examined on the wing upper surface, one on the L.E. flap ahead of the perforated knee, and the remaining three on the main wing aft of the suction surface.

The boundary-layer measurements with the conventional L.E. flaps were confined to the case $\delta_N = 32°$, with T.E. flaps retracted, without suction and with the critical value on the starboard wing at $\alpha = 31°$. The non-dimensional total-pressure coefficients are shown in Fig. 18, and the derived chordwise variations in the boundary-layer thickness, $\delta$, in Fig. 19.

When comparing the curves in Fig. 18 without and with suction, some allowance is necessary for thinning due to boundary-layer withdrawal. A comparison between the two cases at $\alpha = 11{\cdot}8°$, $x/c = 0{\cdot}166$ suggests a change of boundary-layer thickness of about 0·02c.

At $C'_Q = 0$, significant boundary-layer thickening can be detected at an incidence as low as 11·8° towards the rear of the wing. By $\alpha_w = 21°$, this effect had spread forwards to the knee of the L.E. flap, and tufts showed severe flow disturbances from the knee to the wing trailing edge. The flow is seen to have collapsed on this wing by $\alpha_w = 23{\cdot}4°$. From the corresponding $C_L$ *vs* $\alpha_w$ curves (Fig. 13a) it is apparent that the presence of thick, feeble boundary layers towards the rear of the wing had little overall effect, the major lift loss and drag increase occurring only with the onset of full separation from the vicinity of the L.E. flap knee.

In the presence of suction, the thickening and degeneration of the boundary layer with increase of incidence proceeded at a much reduced rate. The beneficial influence of suction was naturally greatest near the L.E. flap knee. This was also consistent with the tendency for flow separations in the presence of suction to appear initially towards the wing trailing edge. Once again, however, major adverse effects on lift and drag did not occur until the sudden collapse of the boundary-layer flow from the flap knee, at $\alpha_w = 31°$.

4.2.4. *The effect of suction-surface arrangement on minimum suction rates and suction power requirements.* In general, the results achieved with suction boundary-layer control for high lift correlated in terms of the suction flow rate required to achieve attached flow for a given arrangement and test condition[1]. Thus, comparisons between the various suction surface specimens tested, of either forces or pressure distributions, showed good agreement provided that the appropriate minimum suction value, $C'_{Q_a}$, was applied in each case. A comparison between the merits of the different perforation arrangements can therefore be made in terms of $C'_{Q_a}$, together with the associated plenum chamber pressure coefficient $C_{p_c}$, which determines the associated suction power requirements.

The measured variations of $C'_{Q_a}$ with $\alpha_w$ are shown in Fig. 20, for $\delta_N = 32°$ and $\delta_N = 37°$, with the T.E. Fowler flap extended and deflected. The values shown relate to the starboard wing; as noted earlier, higher values were required to achieve attached flow on the port wing, equivalent to an incidence difference of about 2°. For these tests, a smooth aerofoil contour was ensured in the vicinity of the L.E. flap knee, without leaks; the effect of some practical imperfections is considered later (*see* Fig. 14b and Section 4.5).

To ensure consistent calibrations it was necessary (*see* Section 3.2) to seal one or two rows of holes at the front and rear of each specimen, and a $\frac{1}{4}$ inch wide area (measured parallel to the hinge line) at each end of each chamber. Thus, normally, there were $\frac{1}{2}$ inch wide non-porous areas at the positions of the inter-chamber partitions. Checks were made with the inter-chamber sealing doubled in width, and

without sealing; these showed (Fig. 14c) that the normal sealing arrangements had no significant effects on the critical suction coefficient. It seems probable that this was partly because the non-porous areas were aligned not streamwise, but rather normal to the hinge line, thus minimising the spanwise extent of completely unthinned boundary layer. Further checks were made with rows temporarily sealed at the front and rear of the specimens (Fig. 14d); these showed that the chordwise extent of the porous area was not particularly critical, confirming the tests by NASA[2] with distributed suction (through a felt surface) at the knee of a L.E. flap.

At a given open-area ratio, there was no significant effect of variation of perforation size over the range of hole diameters tested. Moreover, as few as four rows of large diameter holes could be used without appreciable penalty. Larger flow requirements were needed with smaller open-area ratios. As shown by Fig. 21, the calculated 'equivalent' inflow velocity ratio at the *rear* of the porous area (*see* Section 3.3) was sensibly constant over the range of open-area ratios tested, at critical flow conditions. It seems reasonable that this ratio might constitute an additional correlating parameter, because of its influence on the critical condition of the boundary layer at the rear of the flap knee. The additional flow requirements with the smaller open-area ratios were associated with higher mean inflow towards the front of the porous area, and could probably be reduced by grading the chordwise spacing of the rows.

The results of the NASA tests[2] on a 35° swept aspect ratio 4·8 wing provided a convenient datum which has been indicated in Fig. 20. Very similar overall effects were achieved as in the present case, with increases from 1·8 to 2·4 in $C_{L_{max}}$ and from 16° to 29° in stalling incidence with distributed suction at the knee of full-span L.E. flaps ($\delta_N = 35°$ streamwise), and part-span T.E. suction flaps. The present results with larger open-area ratios, a practical perforated surface and simple plenum chambers, show suction requirements comparable with those previously achieved with optimised distributed suction through a graded-resistance surface.

In addition to reducing flow requirements, large open-area ratios were essential to minimise suction power requirements, because of the profound effect of open-area ratio on the plenum-chamber coefficients (Fig. 22). For practical applications, a minimum open-area ratio of about 3 per cent seems necessary, ensuring air speeds $v_H$ through the perforations of similar order as the main stream speed $V_o$ (Fig. 21). Although some further increases in open-area ratio might have provided marginal additional benefits in suction power requirements, limits were set by the need to avoid local outflow without introducing a need for further compartmentation.

In fact, the values of $C_{p_{\tilde{c}}}$ with 3·3 per cent open-area ratio were more or less equal to the peak external values of $C_p$ on the flap knee. Thus, further material reductions in suction power necessitated wing shape modifications decreasing the knee curvature, as described in the next section.

### 4.3. *The Effect of Distributed Suction at the Knee of Extending-Area L.E. Flaps.*

4.3.1. *Forces and moments.* As already described (Section 3.1), forces, moments and suction coefficients with the extending-area flaps have been calculated in terms of the increased reference chord and wing area (for undeflected L.E. flaps). The extension gave minor modifications of aspect ratio and thickness-chord ratio; on deflection the L.E. flaps provided a further area extension of nearly 6 per cent chord, the knee radius being some $2\frac{1}{2}$ times greater than for the conventional leading-edge arrangement.

The force and moment characteristics with the full-span extending-area L.E. flaps deflected are shown in Fig. 23 for $C'_Q = 0$ and 0·0024 (the maximum rate available). Other values of $C'_Q$ produced behaviour intermediate between the extremes shown. On comparing Figs. 13 and 23, it is difficult to detect much effect of the chordwise deflected extension on, for example, the value of the lift-curve slope. Below the stall, the effect of the extending-area flaps was mainly confined to static stability changes associated with planform changes. However, there was a clear beneficial effect at $C'_Q = 0$ associated with the larger knee radius, with stalling incidence increases of from 5° to 8° and $C_{L_{max}}$ increases of about 0·3. At $C'_Q = 0{\cdot}0024$ the corresponding increases were somewhat smaller, although the extending-area L.E. flaps were still appreciably superior to the conventional ones. Thus, there was a reduction in the beneficial effects of distributed suction. As with conventional L.E. flaps, the alternative settings of the L.E. flap produced little difference, without or with suction.

Wing tuft studies at $C'_Q = 0$ confirmed a mid-semispan stall, the port wing leading as before. However, deterioration in the condition of the boundary layer was much more gradual than with the basic L.E. flap. Moreover, the initial flow separation now occurred simultaneously over the chordwise extent of the main wing, aft of the L.E. flap, rather than from the knee of the L.E. flap. With suction, the tendency shown with the conventional L.E. flaps towards full-chord separation was accentuated with the extending-area L.E. flaps, with appreciable spanwise drift at the rear of the wing when the T.E. flaps were retracted. In fact, the initial major flow separation definitely occurred towards the rear of the main wing. As at $C'_Q = 0$, the onset of flow separation with increase of incidence was more gradual with the extending-area leading-edge flaps.

In view of the increased tendency towards rear separation with the extending-area L.E. flaps it was not surprising that the application of suction to the knee of the L.E. flaps was less effective than before, relative to the improved datum behaviour at $C'_Q = 0$. In such circumstances, where suction is applied well forward of the critical region, control by boundary-layer suction is much less positive. As one would expect, critical inflow rates were more difficult to assess than before, particularly with T.E. flaps retracted. However, with some repetition, reliable and consistent results were obtained.

4.3.2. *Surface pressure distributions.* Typical variations of surface pressure at the knee of the extending-area L.E. flap are shown in Fig. 24. As for the conventional L.E. flaps (Fig. 15) the port wing values at 0·466 $b/2$ were more extreme and characteristically peaked, possibly because of tunnel flow characteristics as discussed in Section 4.2.2. The starboard wing was again more suitable for detailed measurement of critical inflow rates and did not appear to be affected by the port-wing flow separations. The chosen position of the main chordwise traverse, at $y = 0{\cdot}656\ b/2$, was still generally representative of the prevailing conditions on this wing at onset of stall.

The substantial beneficial effect of increased knee radius and length on the suction peaks at the knee of the L.E. flaps can be seen by comparing Figs. 15 and 24, the typical change in $C_p$ being approximately 3 (e.g. from $-9$ to $-6$). Similar effects can be seen generally on the main chordwise pressure distribution (Fig. 25) the extending-area configurations exhibiting smaller L.E. peaks and reduced gradients at a given incidence.

With the T.E. flaps retracted, the T.E. pressure tended to diverge, as with the conventional L.E. flaps, confirming the deterioration of the boundary-layer condition.

4.3.3. *Boundary-layer investigations.* With the extending-area L.E. flaps, boundary-layer traverses were again made at $y = 0{\cdot}656\ b/2$ on the starboard wing. In this case, measurements were taken with the T.E. Fowler flaps both extended and retracted. The non-dimensional total-pressure coefficients are shown in Fig. 26, and the derived chordwise variations of boundary-layer thickness are given in Fig. 27. The suction flow rate used in each case was the critical rate for the starboard wing at $\alpha = 32{\cdot}8°$.

At $C'_Q = 0$, and T.E. flaps retracted, significant boundary-layer deterioration was evident towards the wing trailing edge at $\alpha = 19{\cdot}4°$, but there was a strong favourable influence due to the reduction of suction peaks and of adverse gradients at the wing L.E., which can be seen on comparison with the conventional L.E. flaps case (Fig. 18). There was clear indication of a substantial degree of flow separation at the trailing edge before the leading-edge knee boundary layer thickened and separated, and once again the effects on the pressure distributions and overall forces were small prior to the development of the knee separation.

The effects of suction were similar to those for the conventional L.E. flaps, the boundary-layer thickening with increase of incidence at a reduced rate, particularly near the L.E. flap knee, with consequent strengthening of the tendency towards rear separation at an elevated incidence.

With the T.E. flaps extended and deflected, the boundary-layer behaviour was significantly changed, with much reduced rate of growth towards the rear of the wing. Without suction, the initial major flow separation was definitely associated with the L.E. flap knee. With suction, the position was less clear, but again there was rather stronger evidence of a L.E. knee separation.

These results were consistent with the tuft studies and confirmed that the more powerful L.E. device was more likely to lead to T.E. separations, particularly with retracted T.E. flaps. In these circumstances

it was clear that the efficiency of L.E. flap knee suction would be impaired and the definition of critical suction inflow rates would tend to become more difficult, at least with T.E. flaps retracted.

4.3.4. *The effect of suction-surface arrangements on minimum suction rates and suction power requirements.* The variation of starboard wing minimum inflow rates with extending-area L.E. flap and T.E. flap extended are shown in Fig. 28 for the basic wing (smooth knee, no vortex generators) at two L.E. flap settings. At a given incidence, the flow requirements were substantially reduced relative to the conventional L.E. flap arrangement (Fig. 20), but the increment in stalling incidence relative to the case $C'_Q = 0$ was smaller. The effectiveness of distributed suction again did not depend critically on the precise chordwise extent of the perforated region, within limits; from power considerations the larger chordwise extent was therefore naturally preferable.

The corresponding variation of chamber pressure coefficient is shown in Fig. 29. Comparison with the conventional L.E. flap results (Fig. 22) shows a clear advantage of the larger knee radius. It must be noted that, because of the greatly increased chordwise extent of the perforated area, the usual extending-area specimen (specimen G, 1·75 per cent open-area ratio) had a total open-area which was 50 per cent greater than that of the conventional flap specimen with the largest open-area ratio (3·3 per cent). Comparison with the external suction peak values, however, showed that there was some scope for further improvement. With an even larger total open-area (specimen H, open area ratio 5·3 per cent, total open-area 4·6 times the largest 'conventional' open-area), chamber pressure coefficients were reduced still further, virtually to the limit set by the external static pressures. However flow calculations suggest that some outflow may occur at the front of this specimen at the lower incidences and flow rates, confirming the existence of an upper limit to the open-area which can be used with the single plenum chamber preferable for simplicity.

4.4. *The Effect of Vortex Generators.*

Particularly with the more powerful extending-area L.E. flaps, the favourable effects of L.E. knee suction seemed likely to be limited by the increased tendency towards rear separation. In contrast with blowing boundary-layer control, where some latitude in choice of slot position is available with moderate penalty[1,12], the underlying mechanism of flow separation control by suction implies greater sensitivity to the chordwise position of the porous regions. As it was not practicable to incorporate additional boundary-layer control further aft on this model, it was decided to examine how much improvement could be achieved by the addition of vortex generators on the main wing aft of the suction region. Two arrangements of co-rotating vortex generators were tried, suitably aligned to allow for local stream direction. The more effective configuration (*B*, Fig. 9b) entailed 43 elements per wing, located at 20 per cent wing chord close behind the L.E. flap knee.

In general, the vortex generators produced at most small favourable effects (Fig. 30), with small corresponding reductions in minimum suction rates with the T.E. flaps deflected (Fig. 32). With the T.E. flaps retracted, tufts showed that the vortex generators considerably delayed the onset of flow disturbances over the main wing, particularly at $C'_Q = 0$. With the T.E. flaps extended and deflected, the effects were similar and persisted up to the stall. Generally, there was a marked reduction in the spanwise drift of the boundary-layer, otherwise present on the main wing.

Boundary-layer profiles on the main wing aft of the vortex generators show that at $C'_Q = 0$, major reductions in boundary-layer thickness were achieved at the higher incidences, with T.E. flaps retracted or extended and deflected. Boundary-layer traverses with suction were made at the appropriate value of $C'_{Q_a}$ at $\alpha = 32{\cdot}8°$ for each case. With T.E. flaps retracted this was slightly greater with than without vortex generators, but with the T.E. flaps extended and deflected it was substantially less. ($C_Q$ reduced by 0·0005.) Fig. 27 shows the much reduced rate of growth of the boundary-layer with incidence with vortex generators fitted, and the distinct reduction in boundary-layer thickness at the higher incidences.

4.5. *The Effect of Surface Imperfections.*

In an aircraft application, the inherent practical difficulties of a movable control surface imply the likelihood of various types of physical discontinuities, such as steps running spanwise across the wing,

and also leaks between lower and upper surfaces. The sensitivity of the suction arrangements to practical imperfections were examined during the tests with the conventional L.E. flaps (Fig. 14b), and further checks were made with the extending-area L.E. flaps (in the presence of type B vortex generators).

The introduction of a downward step ahead of the porous specimen on the conventional L.E. flap (Fig. 4), of either 0·072 inch or 0·050 inch height (0·0019 $c$ and 0·0013 $c$ respectively), merely changed the value of $C'_{Q_a}$, without materially affecting the overall forces and moments at attachment (Fig. 14b). The increases in $C'_{Q_a}$ with the smaller step (*see* Table below) amounted to about 0·0005, and did not appear to depend greatly on the perforation pattern. Correspondingly larger increases were found with the larger step.

*Starboard Wing—Small Step*

| Specimen | $\alpha_w$ | $C'_{Q_a}$ no step | $\Delta C'_{Q_a}$ step | Percentage increase |
|---|---|---|---|---|
| B | 28·5 | 0·00145 | 0·00065 | 45 |
| E | 24·6 | 0·00070 | 0·00045 | 65 |
| | 28·5 | 0·00115 | 0·00050 | 45 |
| F | 24·6 | 0·00050 | 0·00040 | 80 |
| | 26·5 | 0·00100 | 0·00060 | 60 |
| | 28·5 | 0·00170 | 0·00025 | 15 |

For the more complex extending-area L.E. flap a wider range of imperfections was appropriate (Fig. 10c). At both $C'_Q = 0$ and $C'_Q = 0{\cdot}0024$, the adverse effects of an inter-surface leak ahead of the knee, or a 'scooped' upward step behind the knee, were considerable (about 0·1 reduction in $C_{L_{max}}$). Sealed chambers or depressions ahead of the knee produced small penalties. In terms of $C'_{Q_a}$ (Fig. 33) the penalties of the leak or scoop were rather larger (about 0·0006) than that of the downward step ahead of the knee tested with the conventional L.E. flap.

4.6. *The Effect of Rain.*

Although preliminary assessments of rain effects were made on the normal (inverted model) rig, it was considered essential that the final evaluation should be made with an upright model, bearing in mind considerations of drop trajectory and the subsequent behaviour of water streaming over the wing surface, some of which would enter the surface perforations. The rain gun allowed coverage of the central part of the starboard wing (*see* Section 3.5). The effect of rain on $C'_{Q_a}$ was assessed for a range of water flow rates, the degree of air flow attachment being judged from the internal plenum chamber pressures*, in the absence of balance and external pressure measurements.

The investigations were confined to the conventional L.E. flaps, with $\delta_N = 32°$, $\delta_R = 35°$. Several perforation arrangements were considered, including a practical arrangement with a downward step ahead of the flap knee. As with the inverted model, the port wing stalled first, and the flow collapse on each wing still commenced at mid-semispan. In the absence of rain, the values of $C'_{Q_a}$ were similar to those measured previously with the model inverted. Care had to be taken to make repeat checks of the 'no rain' value after each rain test, to detect deterioration of the wing surface, as surface sealing tape quickly lost adhesion and lifted, and to check the condition of the flow measuring devices, particularly the ring pitot-static, which was liable to total or partial blockage by water. A check on this during the 'rain on' runs was provided by subtracting the port wing flow (whose ring pitot static was of course dry) from the total flow measured at the orifice plate.

Visual observations indicated that a certain amount of water impinged at the wing leading edge near the stagnation line and streamed round the nose across the porous surface. A proportion certainly

*Some comparisons with force measurements were made during the earlier inverted model tests, to confirm that this method was still valid in the presence of rain contamination.

entered the suction chamber, but no serious accumulation occurred. In the presence of rain, the onset of critical conditions was indicated clearly by changes in the appropriate plenum chamber pressures. Provided the surface tape had not lifted, no difficulty was encountered with the re-establishment of attached flow in the absence of rain.

Some scatter occurred on the various measurements of the effect of rain on $C'_{Q_c}$ (Fig. 34). This may be wholly or in part due to reduced accuracy in the measuring system due to water contamination. Generally, there was a small increase in the flow requirements but the penalty was appreciably smaller than that due, for example, to a surface discontinuity.

*Conclusions.*

Low-speed wind-tunnel measurements of longitudinal forces and moments, surface pressures, boundary-layer profiles and suction flow rates have been described for an aspect-ratio 5, 31° sweptback wing-fuselage model, with distributed suction through a variety of perforated surfaces at the knees of full-span L.E. flaps. With conventional L.E. flaps and full-span T.E. Fowler flaps, the application of maximum available suction ($C'_Q \doteqdot 0{\cdot}0025$) increased $C_{L\max}$ from 2·17 to 2·68, the stalling incidence rising from 17·5° to 28·3°, with reduced increments at intermediate values of $C'_Q$. With extending-area L.E. flaps (increased knee radius), $C_{L_{max}}$ rose to 2·47 ($\alpha_{stall} = 25°$) at $C'_Q = 0$, and was further increased to 2·80 ($\alpha_{stall} = 33°$) at $C'_Q = 0{\cdot}0024$. Similar lift increments were achieved with T.E. flaps retracted. To some extent, the effectiveness of L.E. knee suction was limited by an increasing tendency for trailing-edge separations as $C_{L_{max}}$ increased.

The use of a large-scale model in the 24ft tunnel allowed the study of practical perforation sizes (up to 0·047 inch diameter) as well as small numbers of rows (as few as 4). However, the minimum suction rates were only slightly affected by the precise surface perforation design at a prescribed open-area ratio, and were generally comparable with those required in earlier NASA experiments on a similar model with a uniformly-permeable high-resistance surface, despite the present use of practical low-resistance surface, despite the present use of practical low-resistance perforated surfaces and simple plenum chambers compartmented only in the spanwise direction.

The suction requirements did not depend critically on the precise chord-wise extent of the perforated region on the L.E. flap knee, and narrow unperforated regions were acceptable at compartment junctions. Provided local outflow was avoided with the simple plenum chamber desirable for easy construction, significant reductions in suction rates could be achieved by increase of open-area ratio. Thus, with open-area ratios of order 3 to 5 per cent, the associated plenum chamber depressions could be effectively minimised with the limit essentially determined by the external suction peak on the flap knee. By use of extending-area L.E. flaps, with a substantial increase of knee radius, further reductions in chamber depressions were possible (typically to $C_{p_c} = -6$ to $-7$ at maximum $C'_Q$).

Rather surprisingly, hysteresis effects (for increasing and decreasing suction rates at fixed incidence) were almost negligible and the suction requirements were little affected by heavy rain. On the other hand, practical surface imperfections significantly increased the minimum flow requirements, particularly upward steps or local inter-surface leaks.

No major objections have been found to preclude the successful application of suction through perforations for high lift, with reasonable suction flow and power requirements, particularly if large flap knee radii can be provided. Equally, the possible advantages of extending-area L.E. flaps, without suction, appear attractive. In an aircraft application, more emphasis would naturally be necessary on the matching and optimisation of the balance of the L.E. and T.E. high-lift devices. This could possibly lead to the consideration of additional perforated regions at other chordwise positions.

*Acknowledgement.*

Hawker-Siddeley Aircraft (Hatfield) constructed the model and assisted with testing and analysis of results.

---

*Some comparisons with force measurements were made during the earlier inverted model tests, to confirm that this method was still valid in the presence of rain contamination.

## LIST OF SYMBOLS

| | |
|---|---|
| $\rho$ | Local air density, slugs/ft$^3$ |
| $\rho_0$ | Free stream density, slugs/ft$^3$ |
| $V_0$ | Free stream velocity, ft/s |
| $V_s$ | Average inflow velocity through equivalent fully permeable surface, ft/s |
| $V_H$ | Inflow velocity through perforations, ft/s |
| $M$ | Mass flow rate of suction air, slugs/s |
| $c$ | Local wing chord, ft |
| $\bar{c}$ | Aerodynamic mean chord, ft } $c = \bar{c}$ = constant for the untapered wing of this report. |
| $c_f$ | Flap chord, ft |
| $x$ | Distance from L.E. in chordwise direction, ft |
| $\tilde{x}$ | Distance from L.E. along surface in chordwise plane, ft |
| $\tilde{x}_0$ | Value of $\tilde{x}$ at leading edge of suction surface |
| $l$ | Length of suction surface measured along surface in chordwise plane, ft |
| $y$ | Distance from centreline in spanwise direction, ft |
| $b$ | Wing span, ft |
| $z$ | Distance from wing surface, normal to surface, ft |
| $S$ | Gross wing area, ft$^2$ |
| $S'$ | Area of wing spanned by porous surfaces, ft$^2$ |
| $C_Q$ | $\dfrac{M}{\rho_0 V_0 S}$ |
| $C'_Q$ | $\dfrac{M}{\rho_0 V_0 S'}$ |
| $C_{Q_a}, C'_{Q_a}$ | Critical values of $C_Q$, $C'_Q$ |
| $H$ | Total-head pressure, lb/ft$^2$ |
| $H_0$ | Free-stream value of $H$ |
| $p$ | Local static pressure |
| $p_0$ | Free-stream static pressure |
| $h$ | $\dfrac{H-p_0}{H_0-p_0}$ |
| $\delta$ | Boundary-layer thickness, = value of $z$ at $\sqrt{h} = 0{\cdot}99$ |
| $C_p$ | $\dfrac{p-p_0}{H_0-p_0}$ |
| $C_{p_c}$ | Value of $C_p$ in plenum chamber |
| $\chi$ | Open area ratio of perforated surface, = $na$ where $n$ is the number of holes per unit area, and $a$ = area of one hole |

## REFERENCES


| No. | Author(s) | Title, etc. |
|---|---|---|
| 1 | J. Williams and S. F. J. Butler | Aerodynamic aspect of boundary-layer control for high lift at low speeds. R.A.E. Tech. Note Aero 2858 (A.R.C. 24535, AGARD Report 414) (1962). |
| 2 | C. A. Holyhauser and R. K. Martin | The use of a leading-edge area-suction flap to delay separation of air flow from the leading edge of a 35° sweptback wing. NACA RMA 53 J 26 TIB 4020 (1953). |
| 3 | G. E. Cooper and R. C. Innes | The effect of area-suction type boundary-layer control on the landing approach characteristics of a 35° swept-wing fighter. NACA RMA 55 K 14 TIB 4952 (1955). |
| 4 | R. T. Pankhurst and D. W. Holder | *Wind-tunnel technique.* Sir Isaac Pitman and Son Ltd. |
| 5 | H. C. Garner | Lift interference on three-dimensional wings. Chap. III. *Subsonic wind tunnel wall corrections.* AGARDOGRAPH No. 109 (1966). |
| 6 | — | Unpublished test reports. Hawker-Siddeley Aircraft (Hatfield). |
| 7 | — | Royal Aeronautical Society Data Sheets, Aerodynamics. |
| 8 | M. H. L. Waters and L. J. Warren | Tests in the R.A.E. blower tunnel of the air blast system for TSR 2 windscreen rain clearance. R.A.E. Report Mech. Eng. 25 (1963). |
| 9 | W. J. Humphreys | *Physics of the air.* Franklin Institute, Philadelphia (1920). |
| 10 | J. A. Lawford | Calibration of the R.A.E. 24 ft wind tunnel. R.A.E. Tech. Report 65188 (1965). |
| 11 | H. H. Pearcy | A method for the prediction of onset of buffeting and other separation effects from wind tunnel tests on rigid models. AGARD Report No. 223 (1958). |
| 12 | S. F. J. Butler | Low speed wind tunnel tests on a sweptback wing model (Buccaneer Mark I) with blowing at the wing leading edge and blowing over the flaps and drooped ailerons. R.A.E. Tech Report 67223 (1967). |
| 13 | R. C. W. Eyre and S. F. J. Butler | Low speed wind tunnel tests on an A.R.8 swept wing subsonic transport research model with BLC blowing over nose and rear flaps for high lift. R.A.E. Tech. Report 67112 (1967) A.R.C. 29389. |

TABLE 1

*Details of Model*

| | |
|---|---|
| Wing span | 15·75 ft |
| Wing chord (constant across span) | |
| Conventional hinged L.E. flap | 3·15 ft |
| Extending-area L.E. flap | 3·26 ft |
| Wing area | |
| Conventional L.E. flap | 49·60 sq ft |
| Extending-area L.E. flap | 51·35 sq ft |
| Sweepback angle | 31° |
| cg position (conventional L.E. flap) | 0·295 $\bar{c}$ |
| cg position (extending-area L.E. flap) | 0·318 $\bar{c}$ |
| Flap chord | |
| Conventional L.E. flap | 0·13 $c$ |
| Extending-area L.E. flap (at 0° deflection) | 0·16 $c$ |
| T.E. flaps | 0·35 $c$ |
| Fuselage maximum diameter | 1·78 ft |

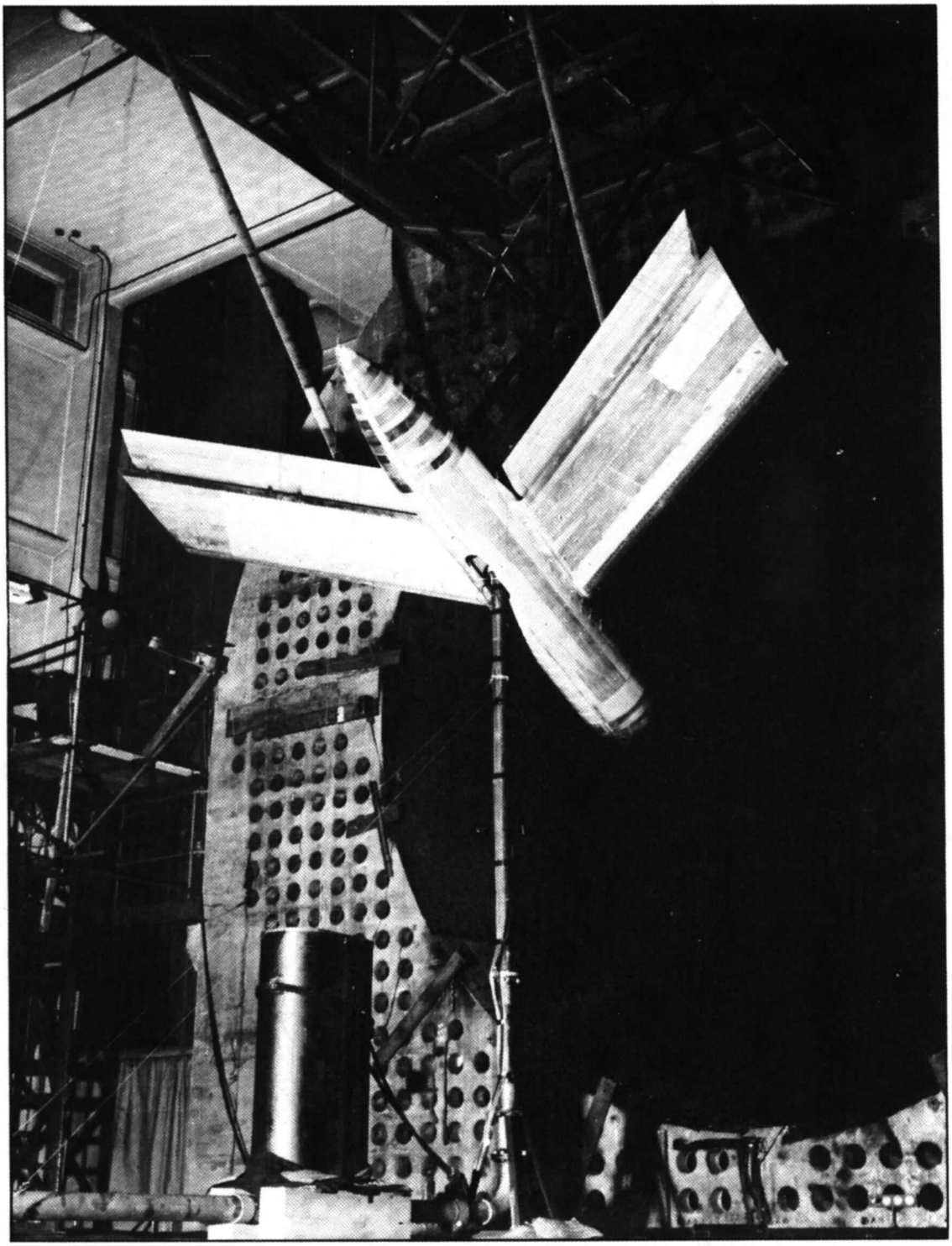

FIG. 1. A.R.5 31° sweptback wing model in R.A.E. 24 ft diameter open-jet tunnel.

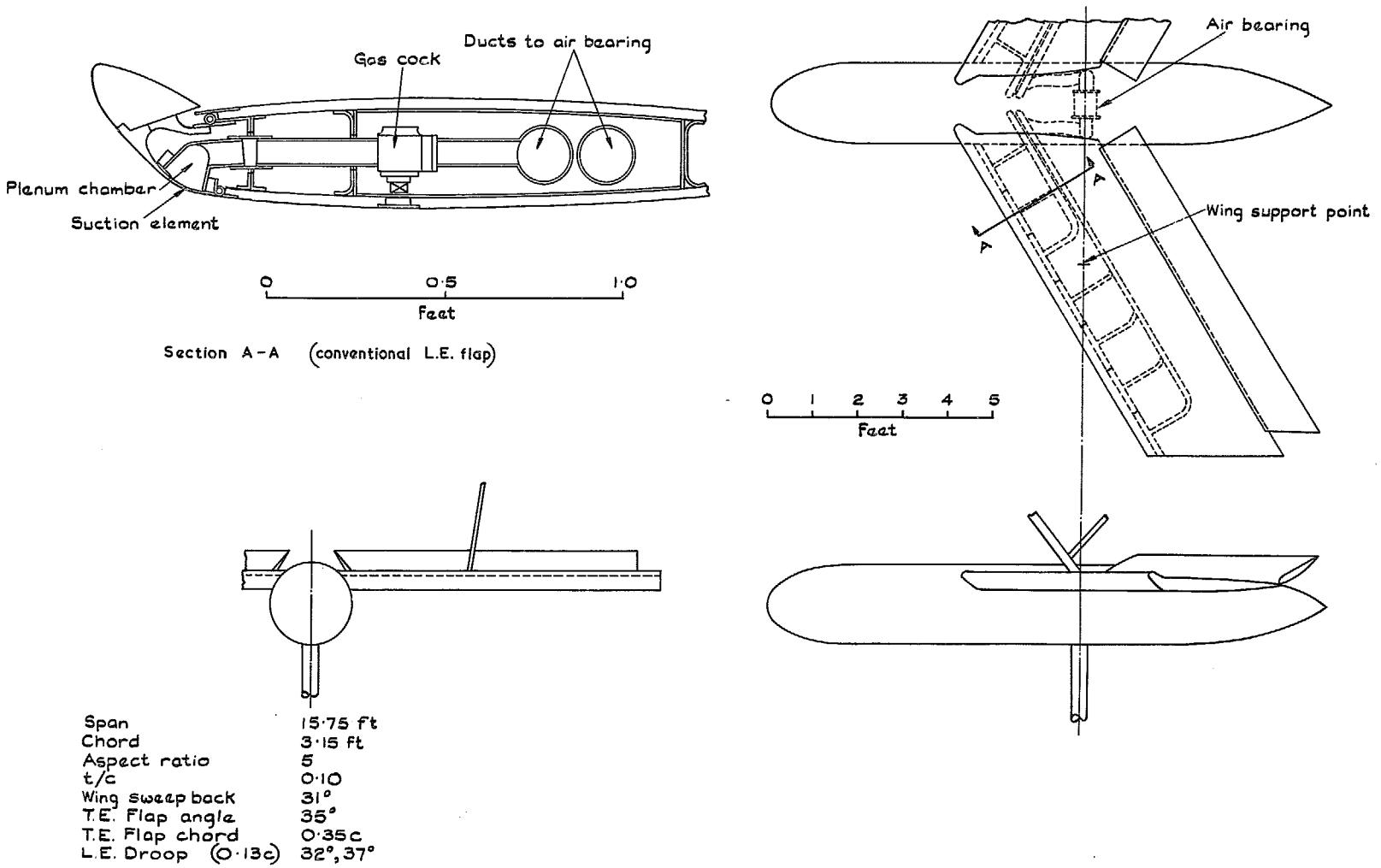


FIG. 2. General arrangement of A.R.5, 31° sweptback wing model with L.E. flap suction.

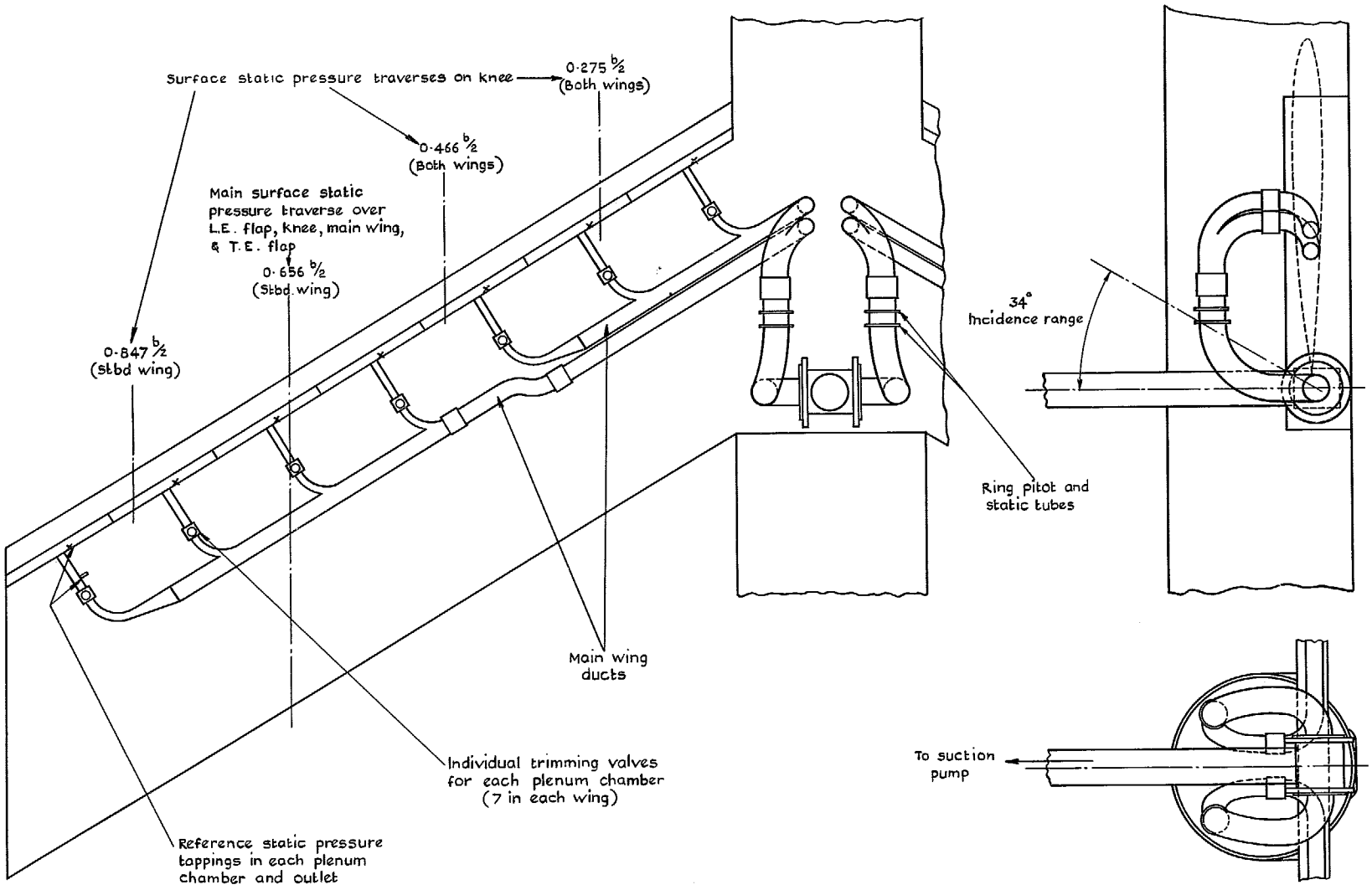


FIG. 3. Details of wing ducting and Instrumentation.

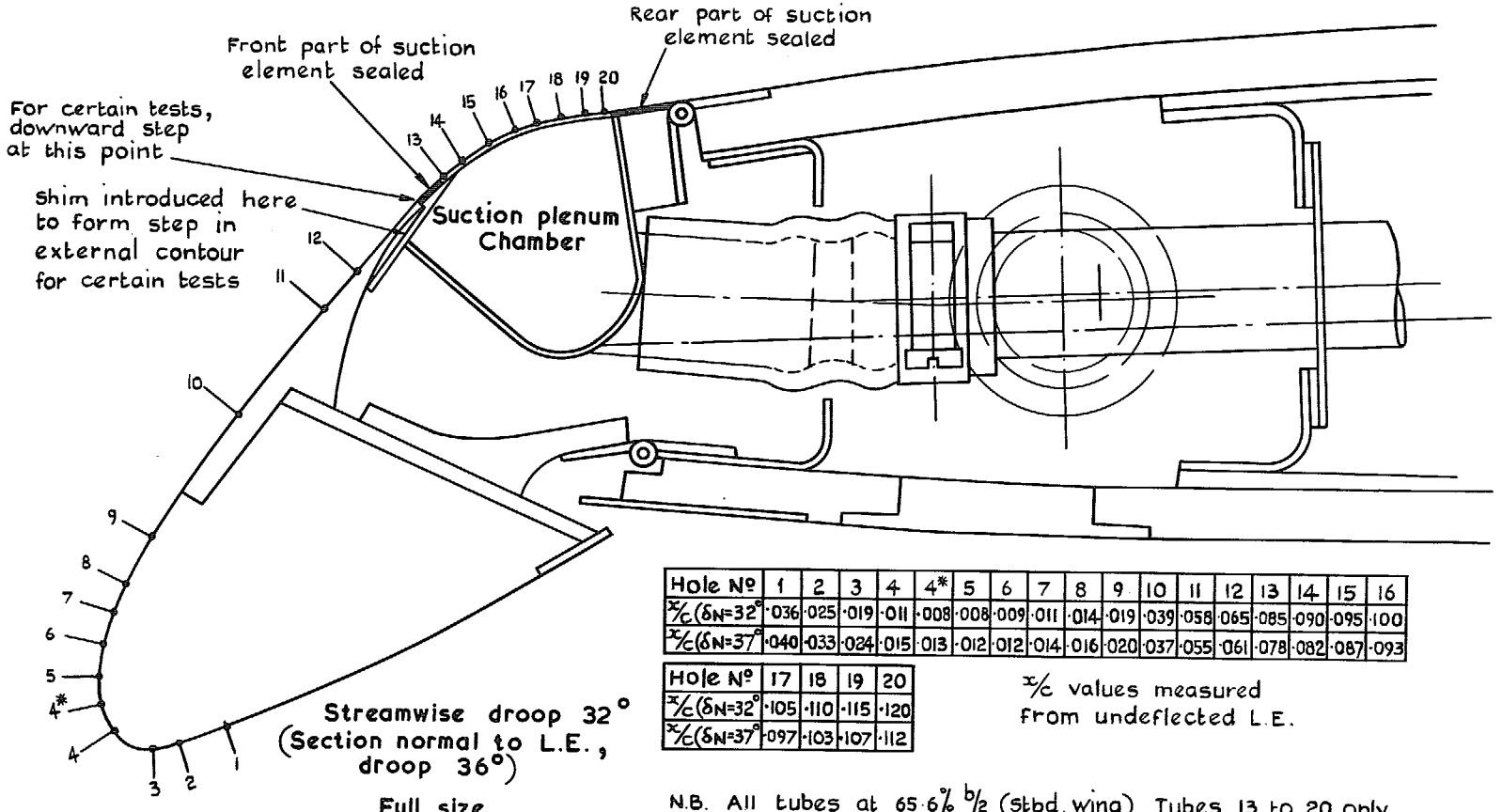


| Hole Nº | 1 | 2 | 3 | 4 | 4* | 5 | 6 | 7 | 8 | 9 | 10 | 11 | 12 | 13 | 14 | 15 | 16 |
|---|---|---|---|---|---|---|---|---|---|---|---|---|---|---|---|---|---|
| x/c (δN=32°) | ·036 | ·025 | ·019 | ·011 | ·008 | ·008 | ·009 | ·011 | ·014 | ·019 | ·039 | ·058 | ·065 | ·085 | ·090 | ·095 | ·100 |
| x/c (δN=37°) | ·040 | ·033 | ·024 | ·015 | ·013 | ·012 | ·012 | ·014 | ·016 | ·020 | ·037 | ·055 | ·061 | ·078 | ·082 | ·087 | ·093 |

| Hole Nº | 17 | 18 | 19 | 20 |
|---|---|---|---|---|
| x/c (δN=32°) | ·105 | ·110 | ·115 | ·120 |
| x/c (δN=37°) | ·097 | ·103 | ·107 | ·112 |

x/c values measured from undeflected L.E.

N.B. All tubes at 65·6% b/2 (stbd. wing) Tubes 13 to 20 only at 27·5%, 46·6%, 84·7%, b/2 (stbd. wing) and 27·5%, 46·6% b/2 (port wing)

FIG. 4. Conventional L.E. flap arrangement.

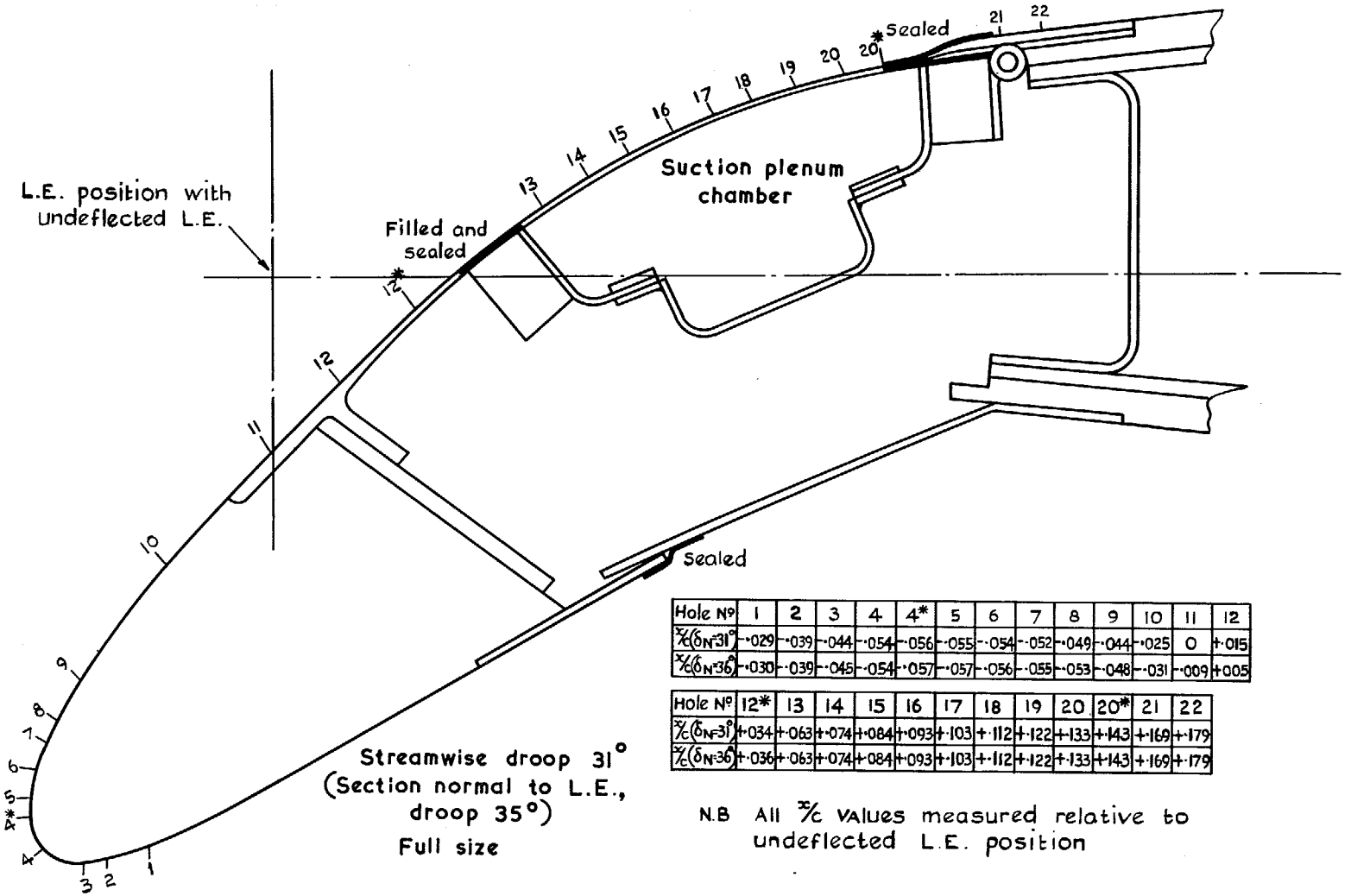


| Hole Nº | 1 | 2 | 3 | 4 | 4* | 5 | 6 | 7 | 8 | 9 | 10 | 11 | 12 |
|---|---|---|---|---|---|---|---|---|---|---|---|---|---|
| %c(δN=31°) | -·029 | -·039 | -·044 | -·054 | -·056 | -·055 | -·054 | -·052 | -·049 | -·044 | -·025 | 0 | +·015 |
| %c(δN=36°) | -·030 | -·039 | -·045 | -·054 | -·057 | -·057 | -·056 | -·055 | -·053 | -·048 | -·031 | -·009 | +·005 |

| Hole Nº | 12* | 13 | 14 | 15 | 16 | 17 | 18 | 19 | 20 | 20* | 21 | 22 |
|---|---|---|---|---|---|---|---|---|---|---|---|---|
| %c(δN=31°) | +·034 | +·063 | +·074 | +·084 | +·093 | +·103 | +·112 | +·122 | +·133 | +·143 | +·169 | +·179 |
| %c(δN=36°) | +·036 | +·063 | +·074 | +·084 | +·093 | +·103 | +·112 | +·122 | +·133 | +·143 | +·169 | +·179 |

FIG. 5. Extending-area L.E. flap arrangement.

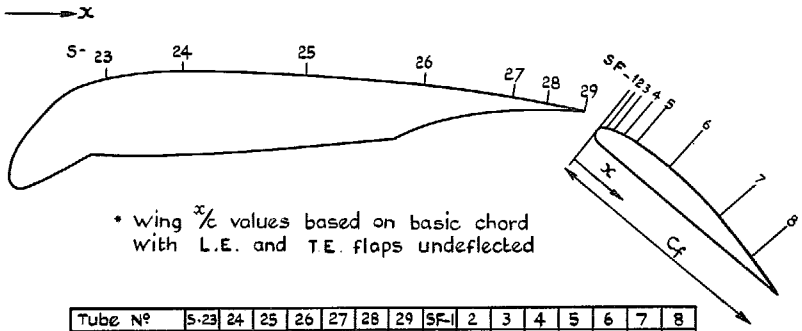


| Tube N° | S-23 | 24 | 25 | 26 | 27 | 28 | 29 | SF-1 | 2 | 3 | 4 | 5 | 6 | 7 | 8 |
|---|---|---|---|---|---|---|---|---|---|---|---|---|---|---|---|
| x/c (Hinged droop) | 0·20 | 0·30 | 0·52 | 0·70 | 0·90 | 0·95 | 1·00 | | | | | | | | |
| x/c (Ext'd droop) | 0·23 | 0·32 | 0·54 | 0·71 | 0·90 | 0·95 | 1·00 | | | | | | | | |
| x/cf (Flaps) | | | | | | | | 0 | 0·02 | 0·05 | 0·10 | 0·20 | 0·40 | 0·70 | 0·90 |

Fig.6 Wing and T.E. flap static pressure details. 65·6% $b/_2$ starboard wing only

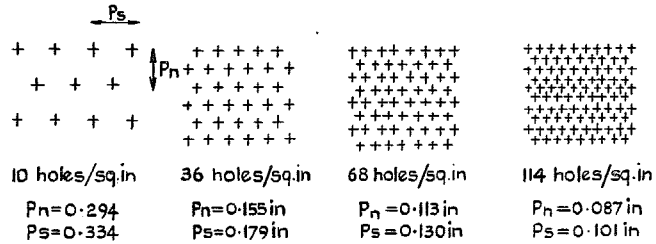


Typical hole centre arrays (3/5 full size)

| Specimen | Holes/sq.in | Hole diam. | Open area | No. of rows | Leading edge |
|---|---|---|---|---|---|
| * A | 10 | 0·047 in | 1·73 % | 4 | |
| B | 36 | 0·025 in | 1·75 % | 7 | Conventional |
| C | 54 | 0·025 in | 2·6 % | 9 | L.E. flap |
| D | 60 | 0·026 in | 3·3 % | 9 | |
| E | 68 | 0·025 in | 3·3 % | 9 | |
| F | 114 | 0·014 in | 1·75% | 13 | |
| G | 32 | 0·026 in | 1·75 % | 18 | Extending-area |
| H | 68 | 0·031 in | 5·3 % | 27 | L.E. flap |

FIG. 7. Details of suction-surface configurations.

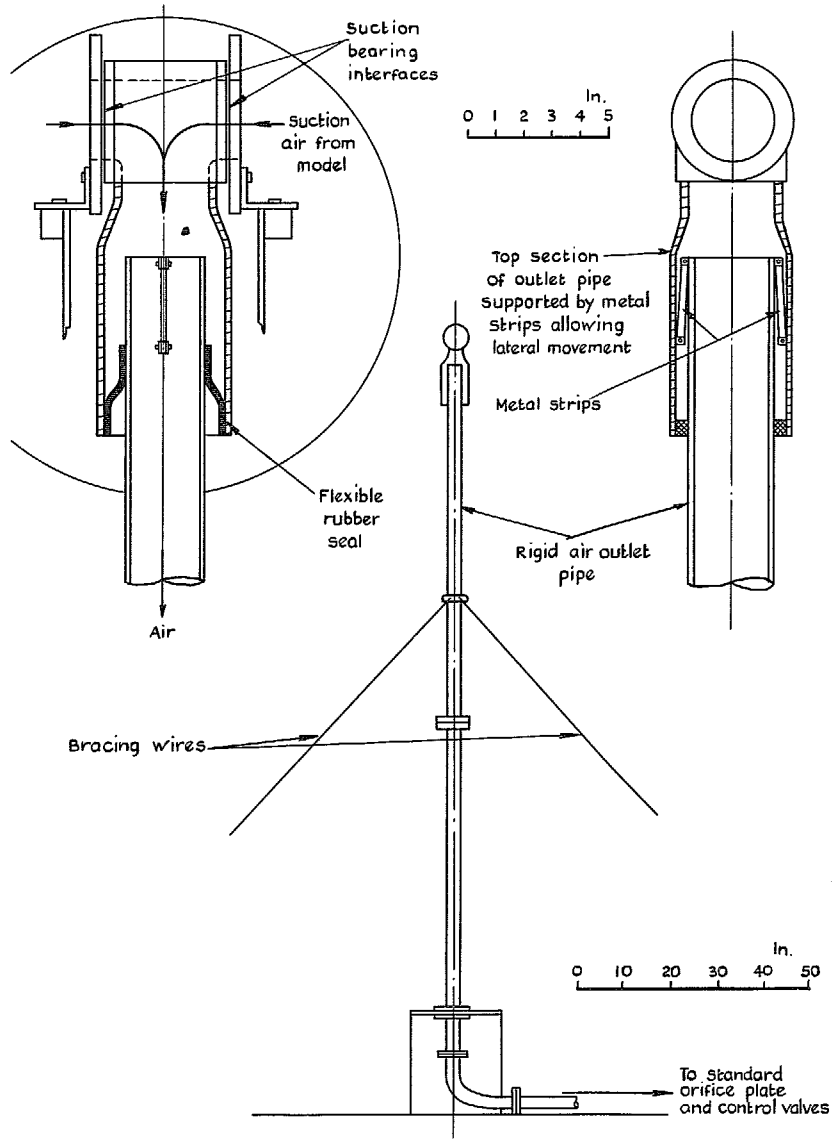


FIG. 8. Details of suction air connector arrangement.

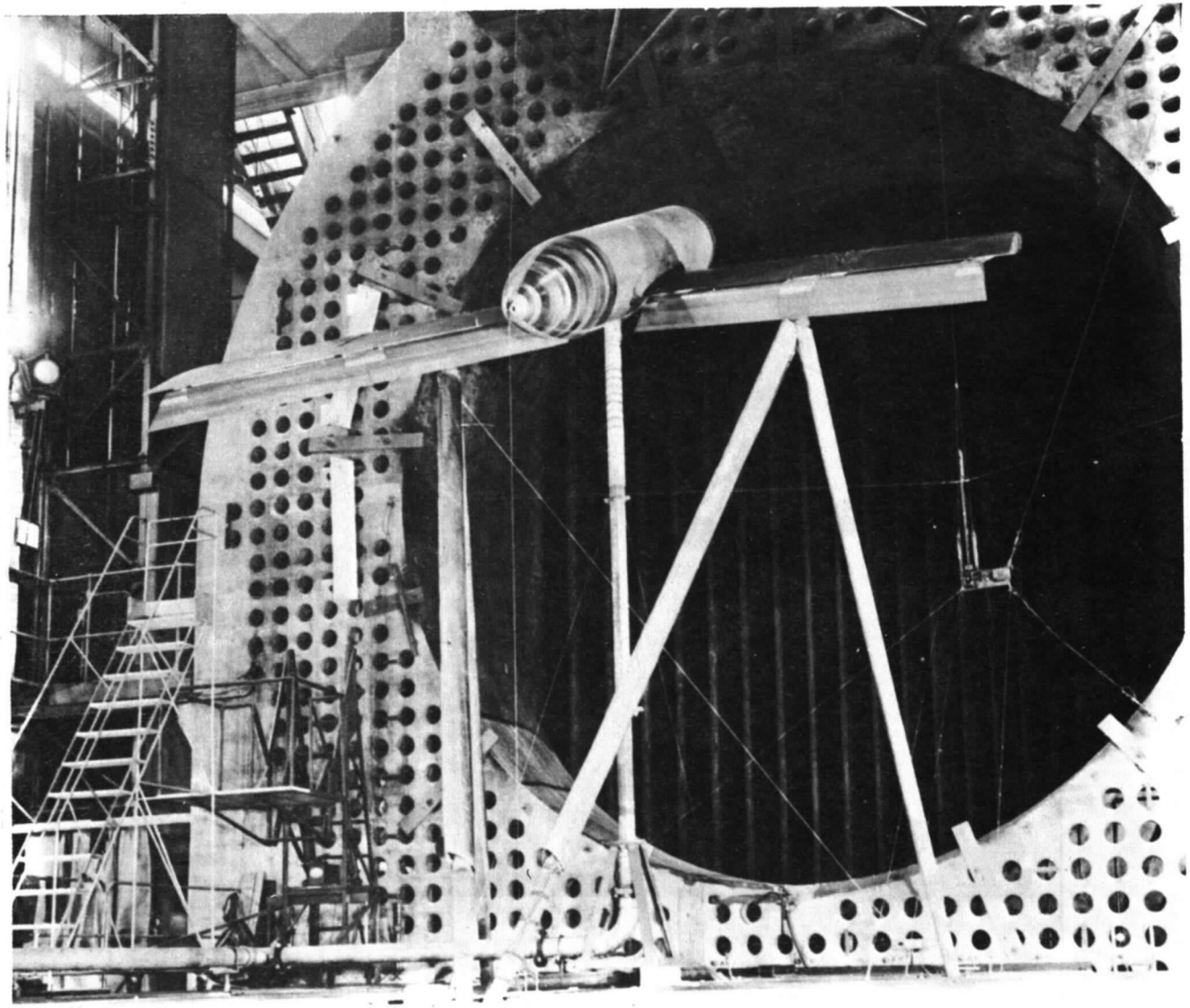

(a) Upright model rig with spray gun in position.

FIG. 9. Arrangement for rain simulation tests.

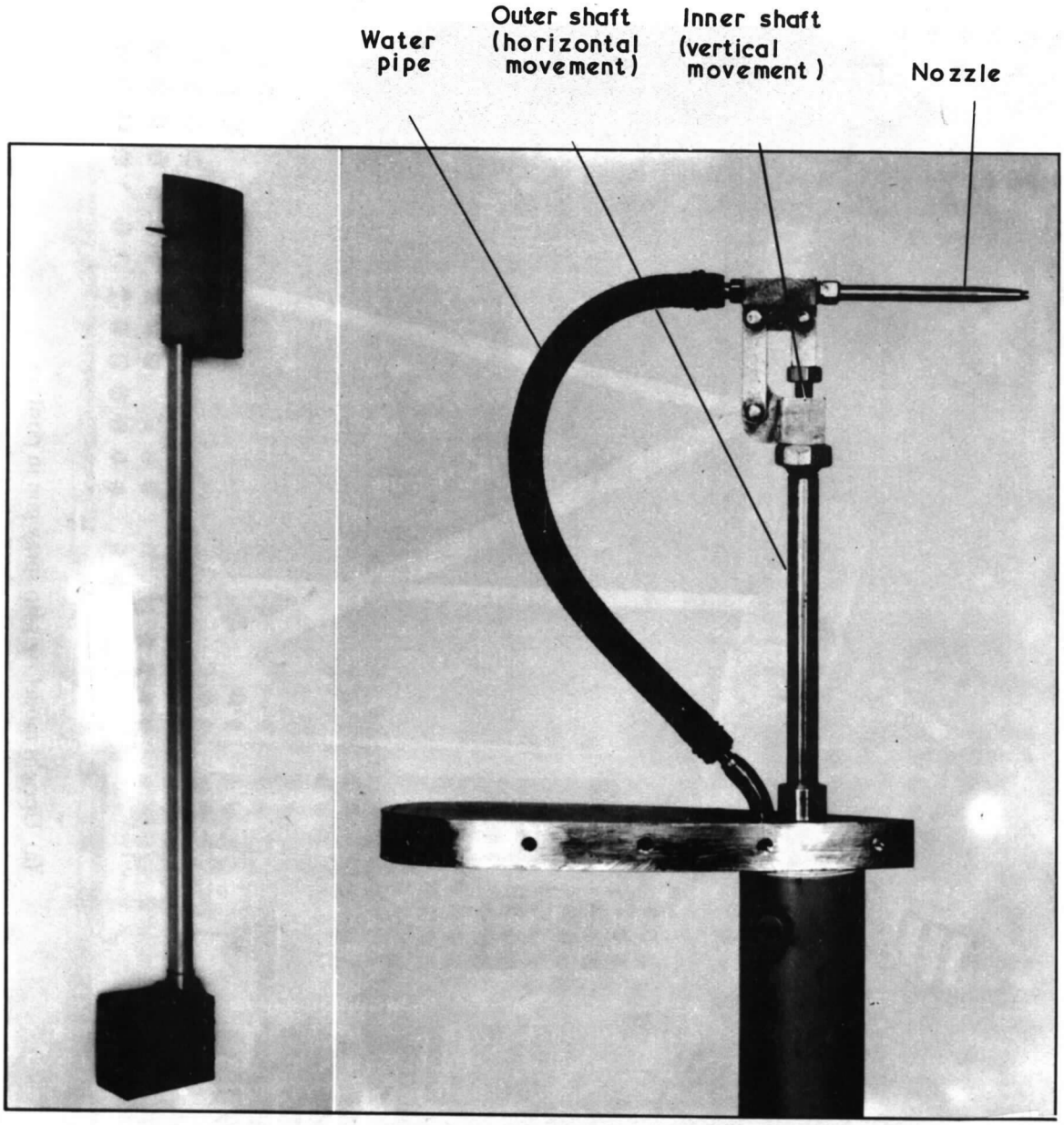


(b) Rain spray gun.

FIG. 9 (cont'd.). Arrangement for rain simulation tests.

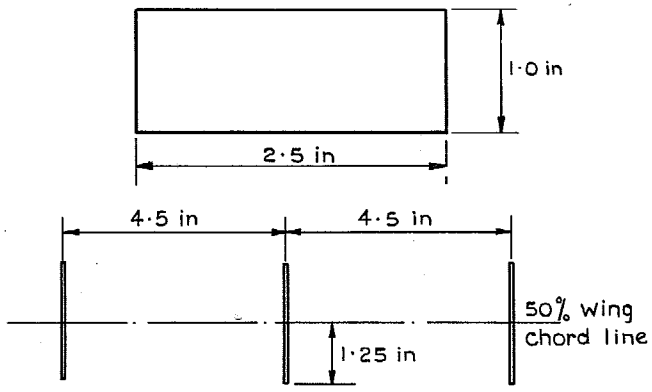


(a) Vortex generators type A (22 elements per wing)

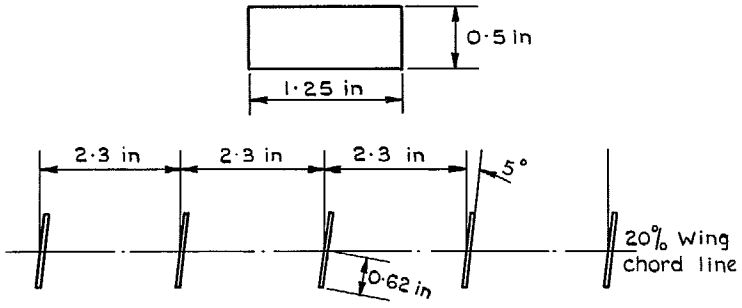


(b) Vortex generators type B (43 elements per wing)

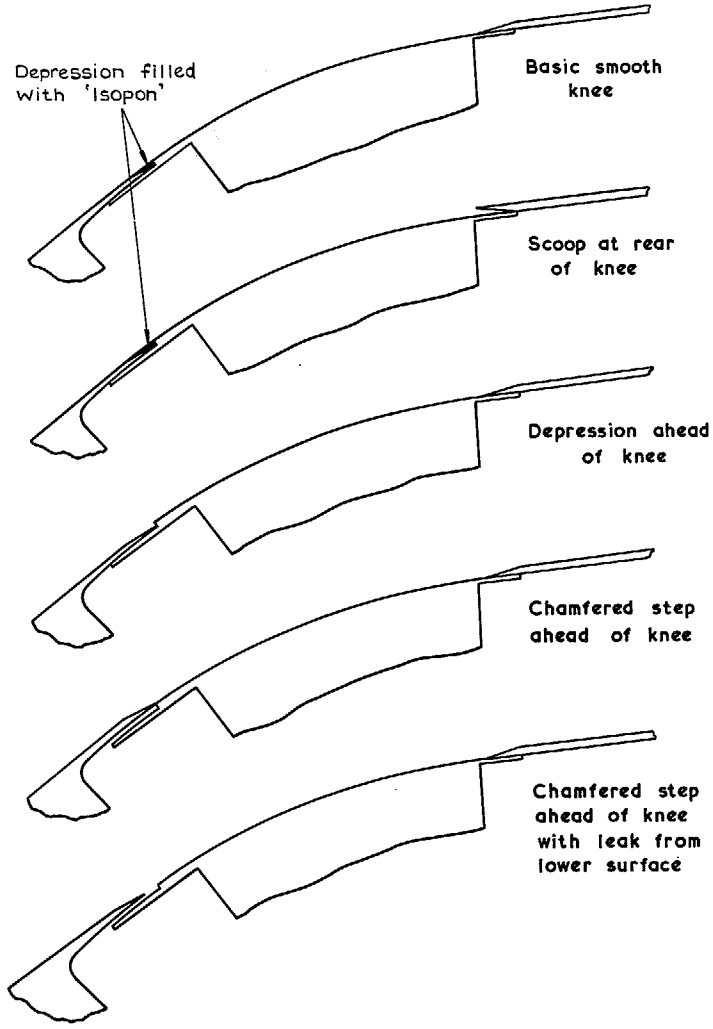


(c) suction surface imperfections for extending area leading – edge flaps

FIG. 10 (cont'd.). Details of vortex generators and suction-surface imperfections.

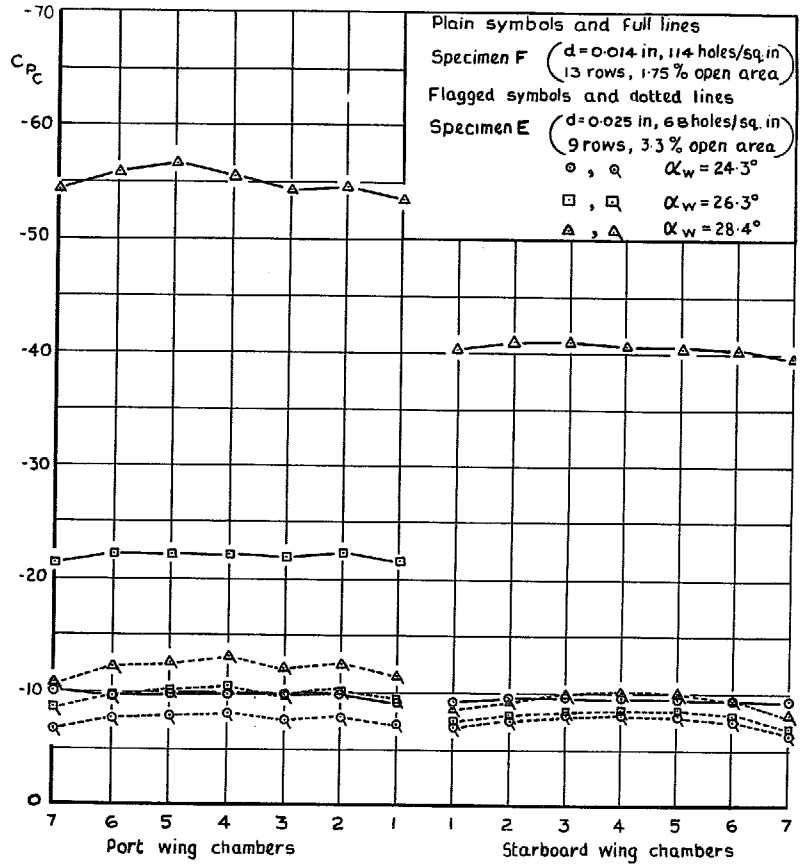


FIG. 11. Typical spanwise variations of plenum chamber pressure coefficient at attachment suction rate. $\delta_N = 32°$, $\delta_R = 35°$.

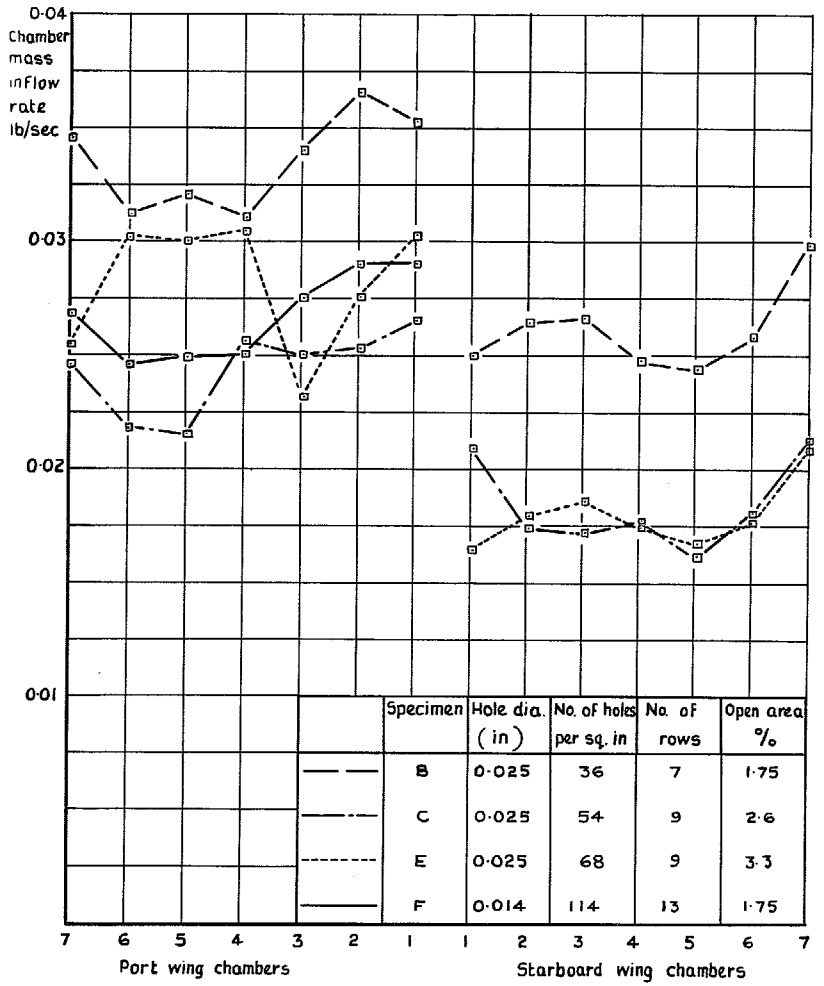


| | Specimen | Hole dia. (in) | No. of holes per sq. in | No. of rows | Open area % |
|---|---|---|---|---|---|
| — — | B | 0·025 | 36 | 7 | 1·75 |
| —·— | C | 0·025 | 54 | 9 | 2·6 |
| ------ | E | 0·025 | 68 | 9 | 3·3 |
| ——— | F | 0·014 | 114 | 13 | 1·75 |

FIG. 12. Typical spanwise variations of mass-inflow rates at attachment suction rate. $\alpha_W = 26·3°$, $\delta_N = 32°$, $\delta_R = 35°$.

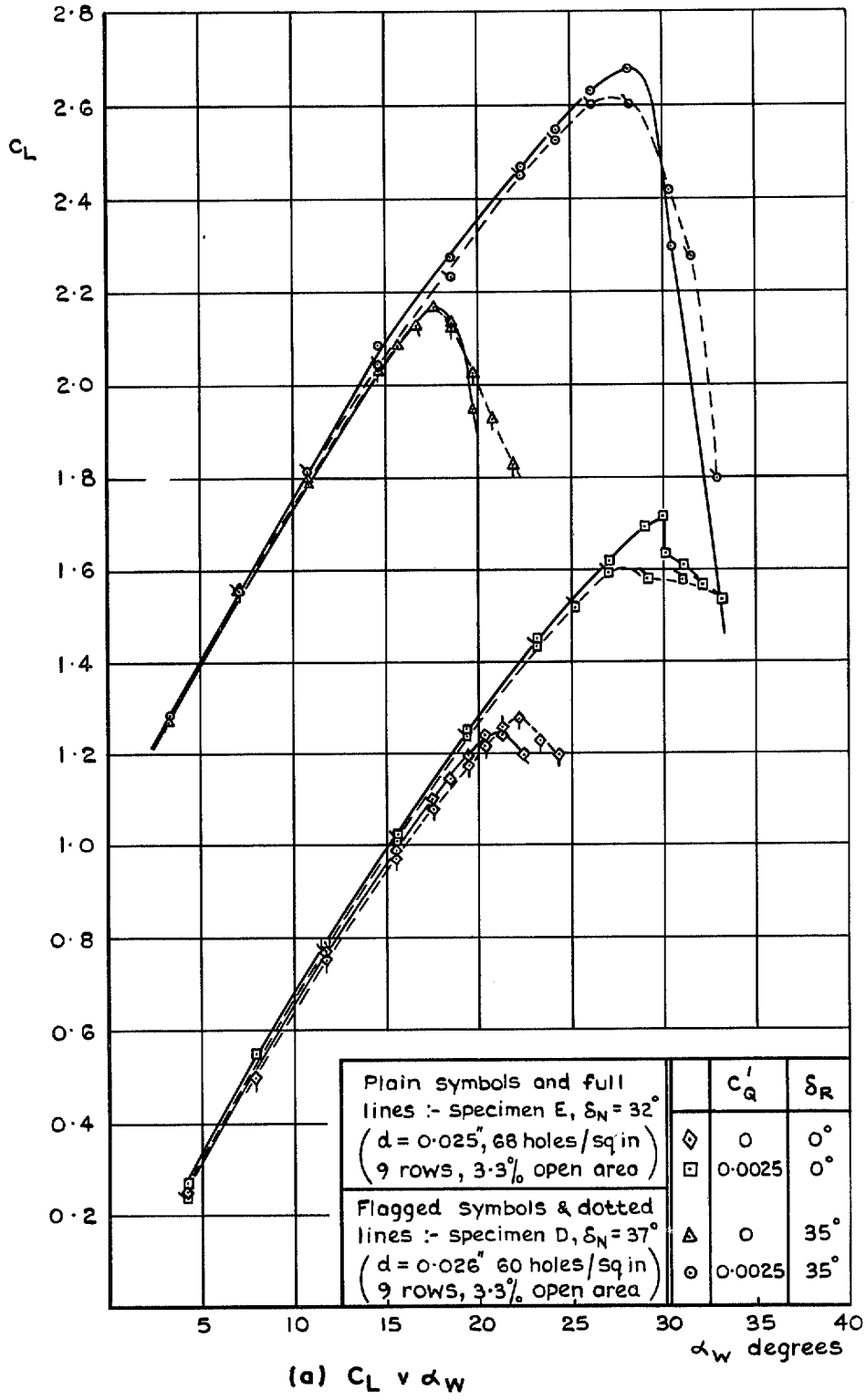


FIG. 13. The effect of distributed suction at knee of conventional L.E. flap on force and moment characteristics.

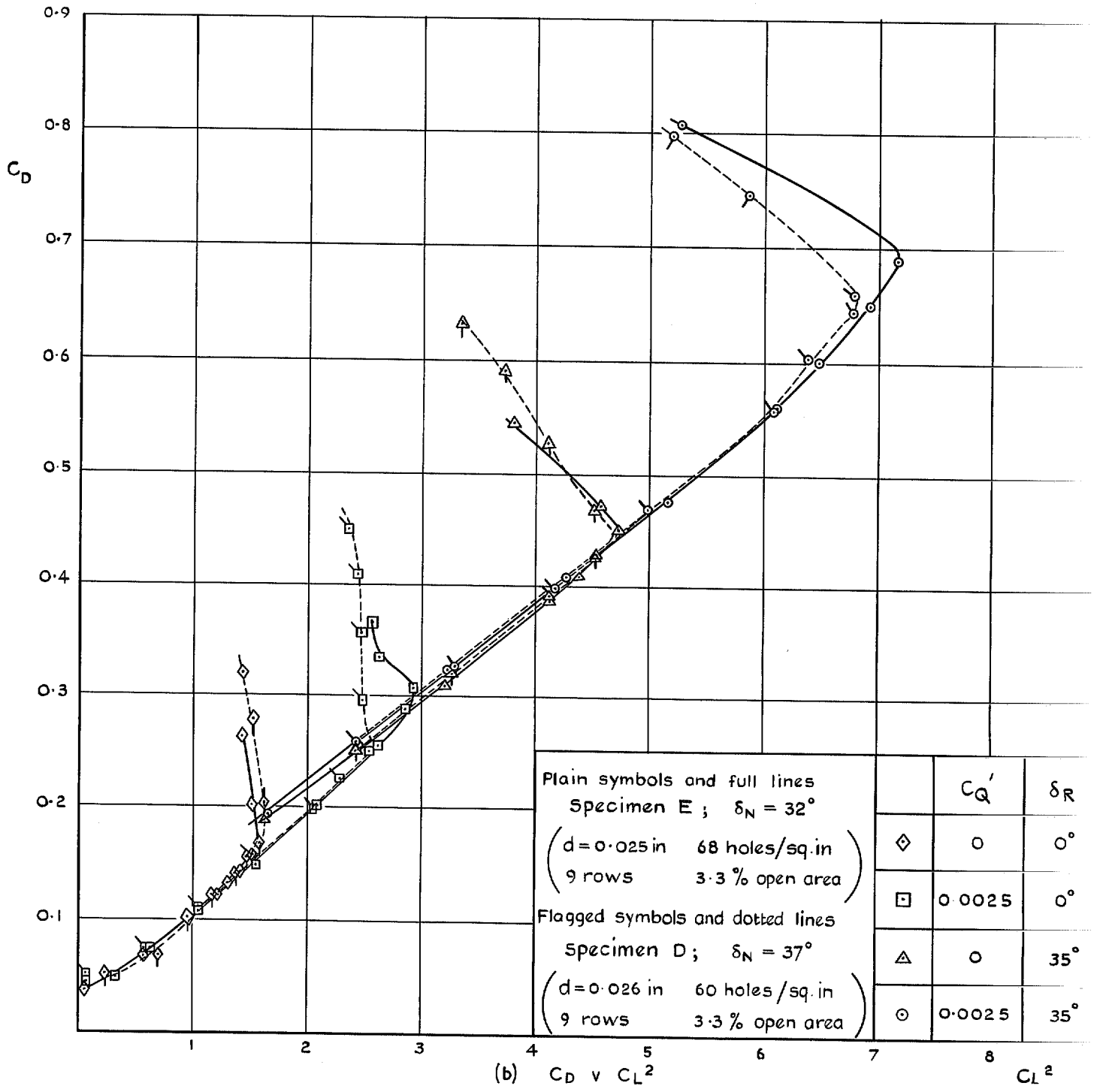


FIG. 13 (cont'd.). The effect of distributed suction at knee of conventional L.E. flap on force and moment characteristics.

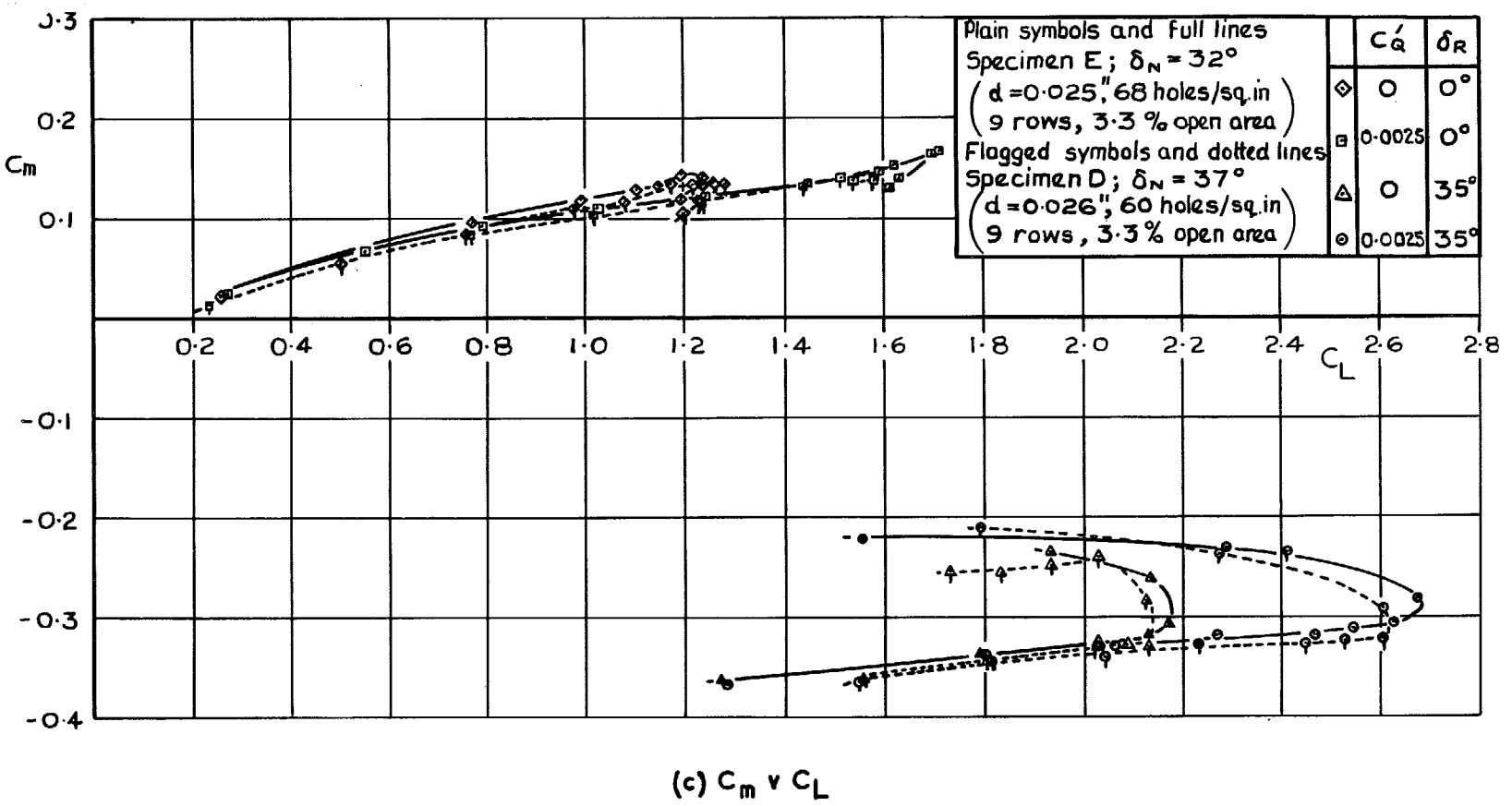


(c) $C_m$ v $C_L$

FIG. 13 (concld). The effect of distributed suction at knee of conventional L.E. flap on force and moment characteristics.

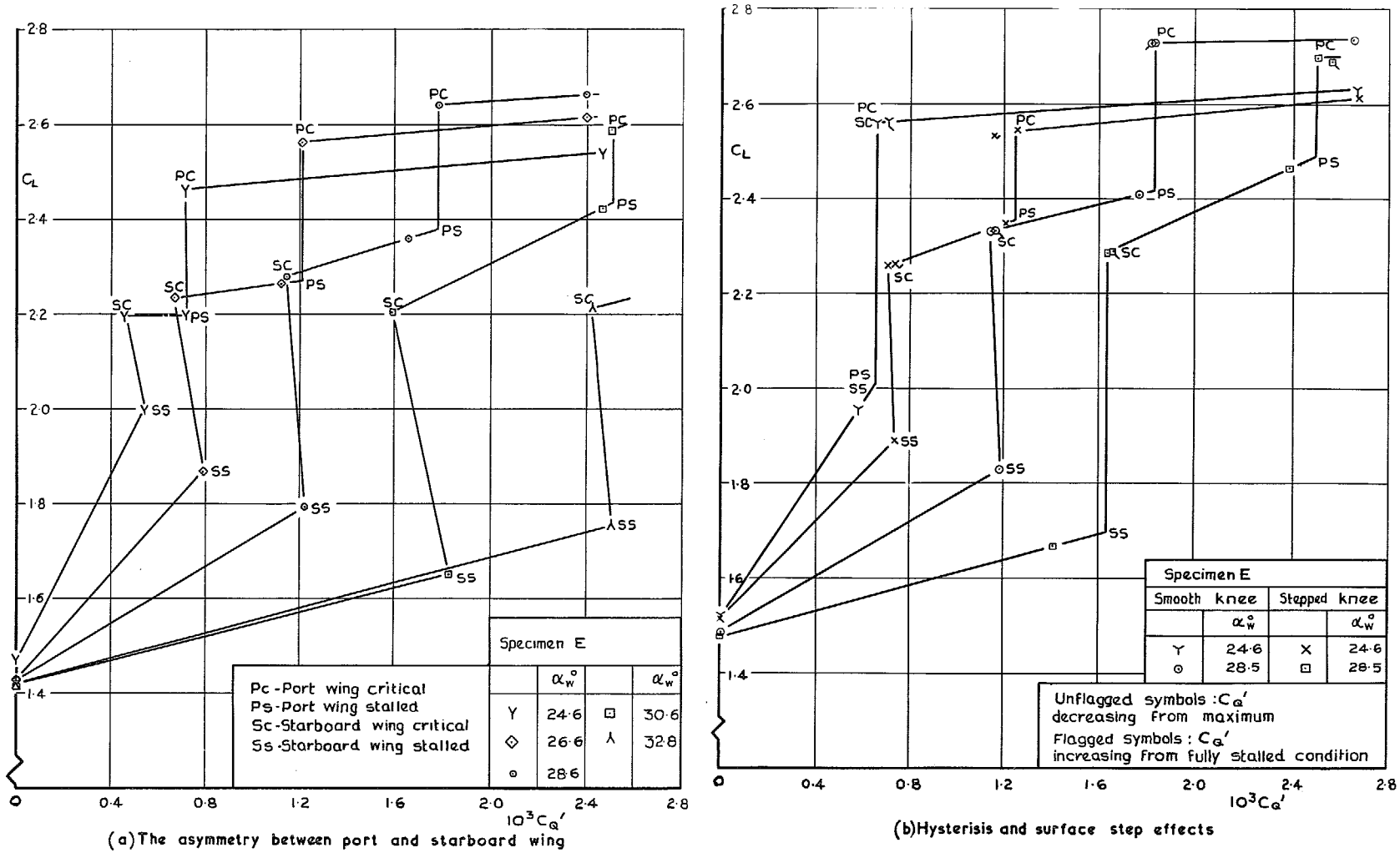


(a) The asymmetry between port and starboard wing

(b) Hysterisis and surface step effects

FIG. 14. Typical effects of distributed suction at knee of conventional L.E. flap on $C_L$ and $C_Q$ at fixed incidence. $\delta_N = 32°$. $\delta_R = 35°$.

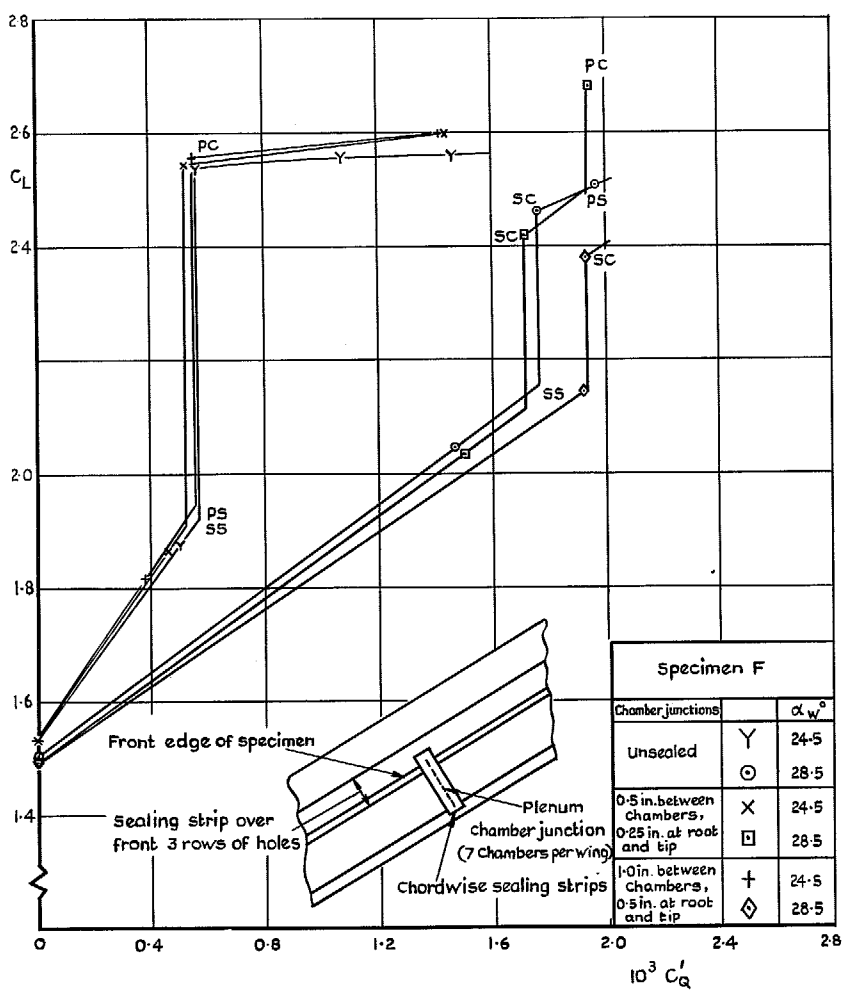


(c) The effects of sealing strips at chamber junctions

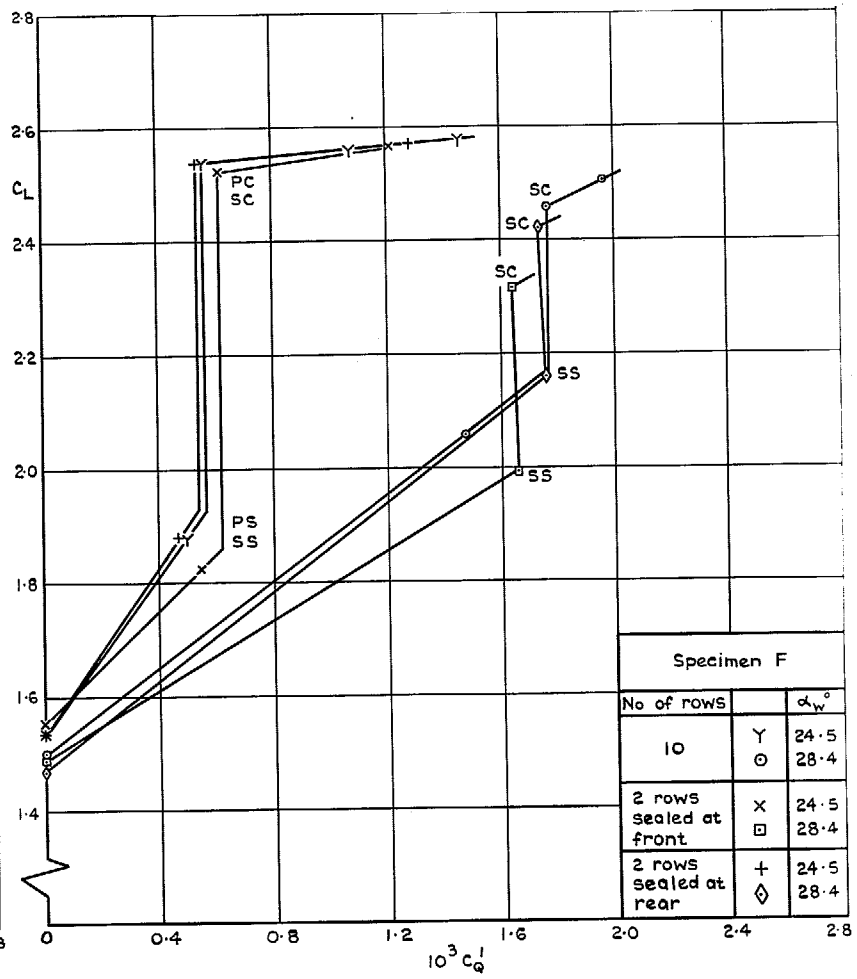


(d) The effect of chordwise extent of perforated surface

FIG. 14 (concld). Typical effects of distributed suction at knee of conventional L.E. flap on $C_L$ and $C_Q'$ at fixed incidence. $\delta_N = 32°$, $\delta_R = 35°$.

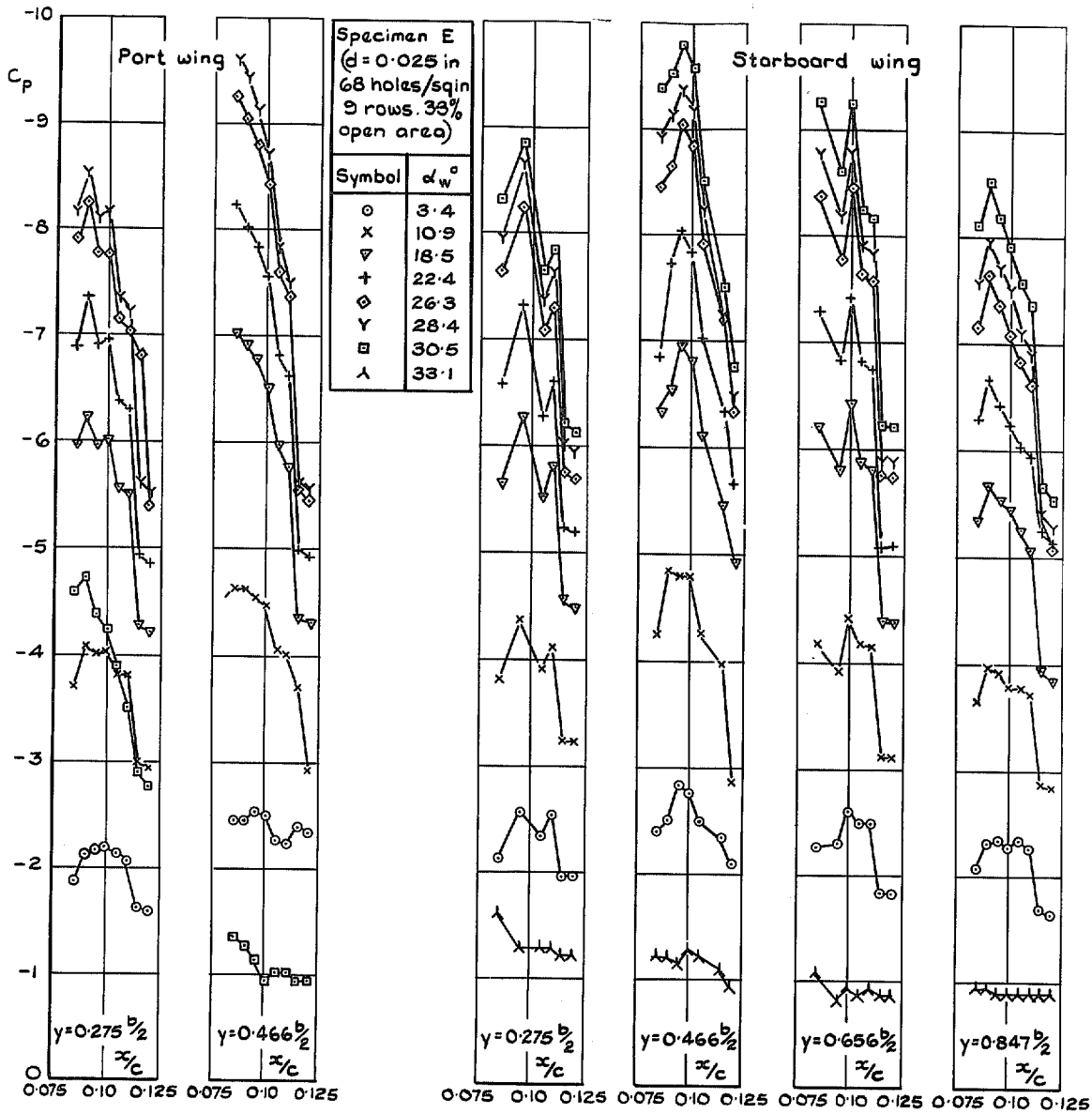


FIG. 15. Spanwise variations of surface pressure at knee of conventional L.E. flap with distributed suction $\delta_N = 32°$ $\delta_R = 35°$: $C'_Q = 0{\cdot}0025$.

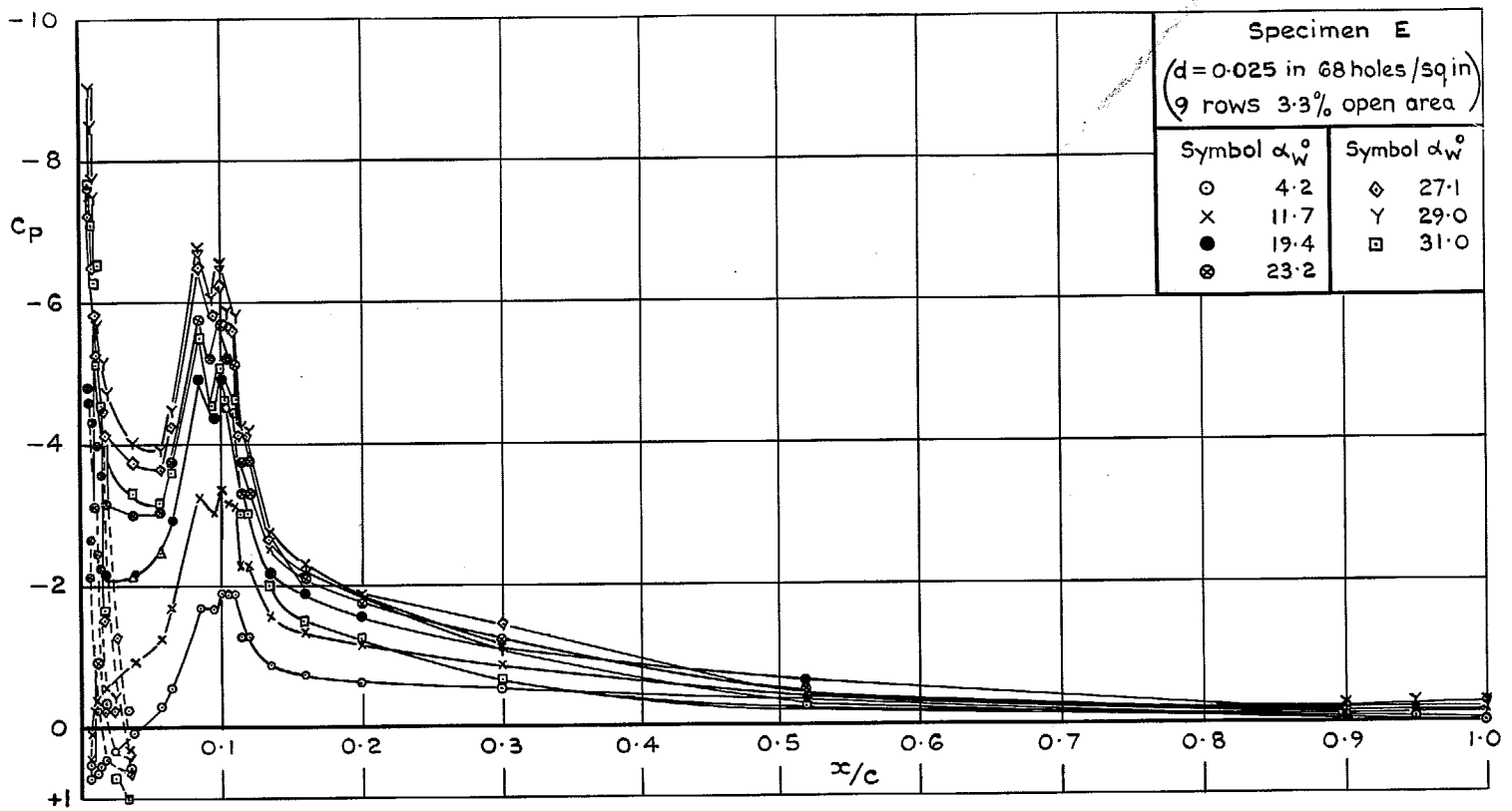


(a) $\delta_N = 32°$ $\delta_R = 0°$ $C_Q' = 0{\cdot}0025$

FIG. 16. The effect of distributed suction at knee of conventional L.E. flap on wing surface pressure distribution (0·656 $b/2$, starboard wing).

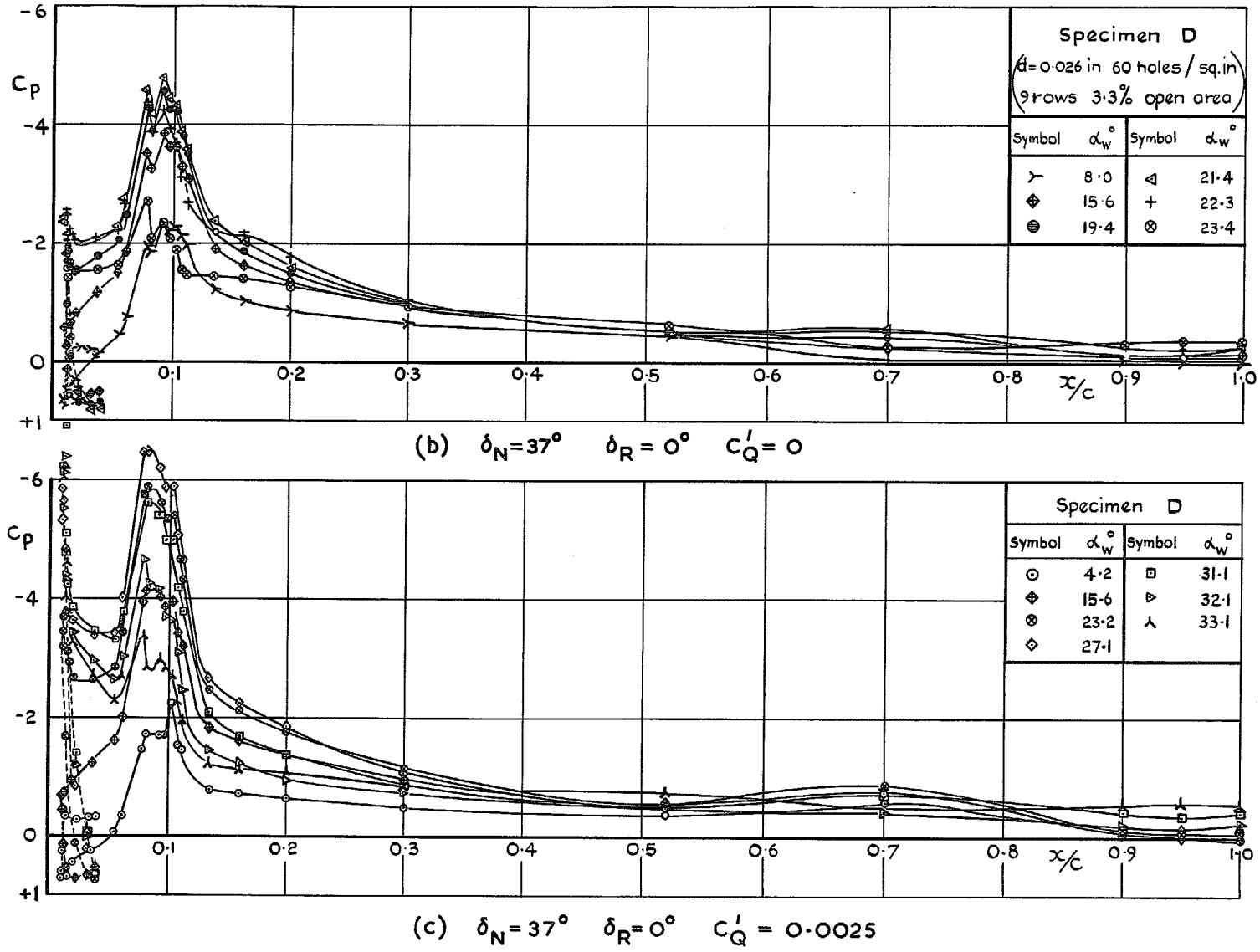


FIG. 16 (cont'd). The effect of distributed suction at knee of conventional L.E. flap on wing surface pressure distribution (0·656 $b/2$, starboard wing).

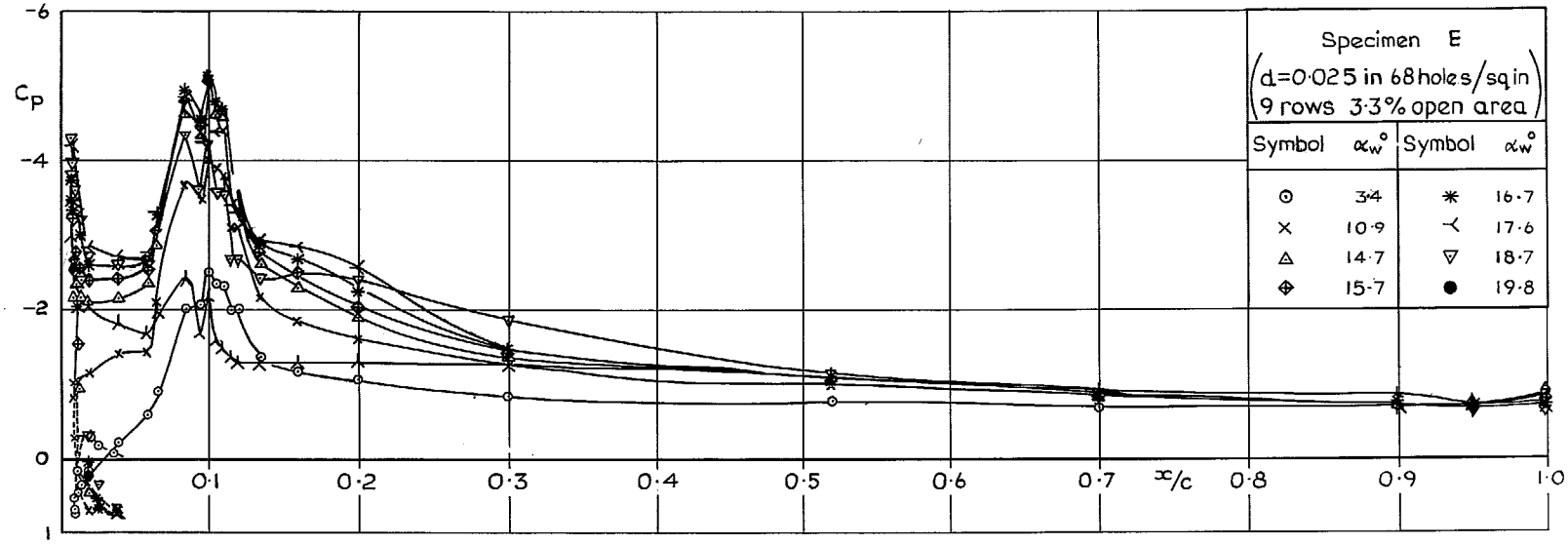


(d) $\delta_N = 32°$. $\delta_R = 35°$ $C_Q' = 0$

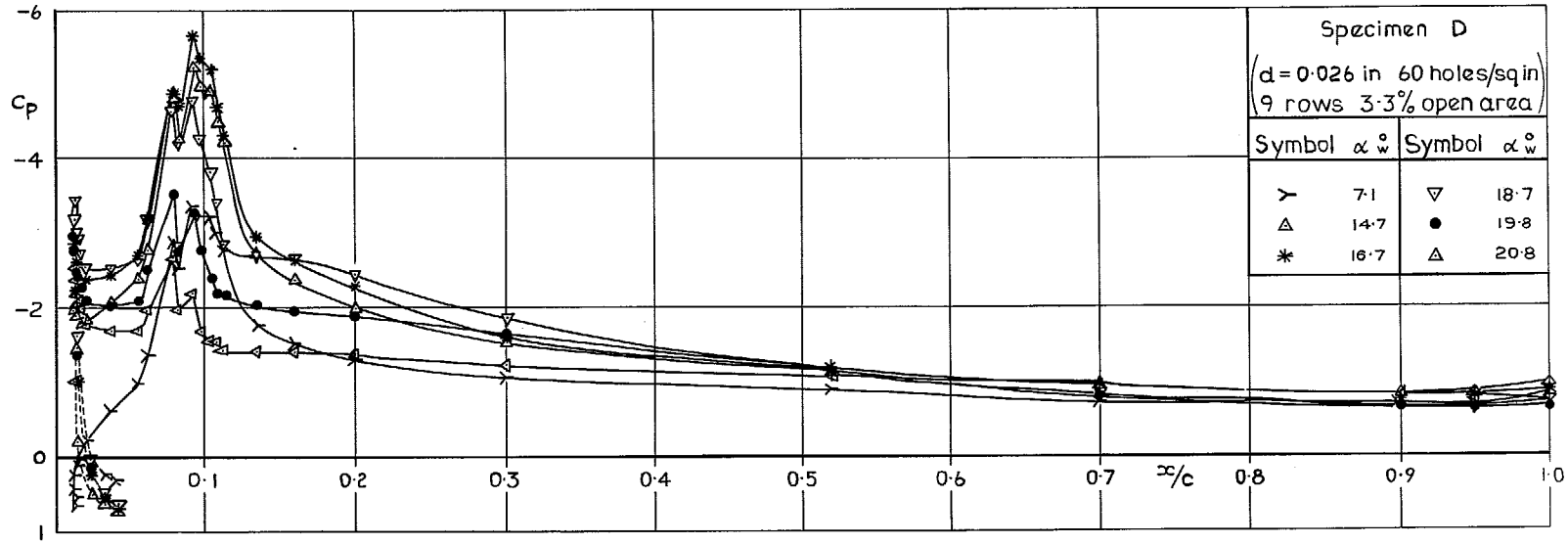


(e) $\delta_N = 37°$ $\delta_R = 35°$ $C_Q' = 0$

FIG. 16 (cont'd). The effect of distributed suction at knee of conventional L.E. flap on wing surface pressure distribution 0·656 *b*/2, starboard wing.

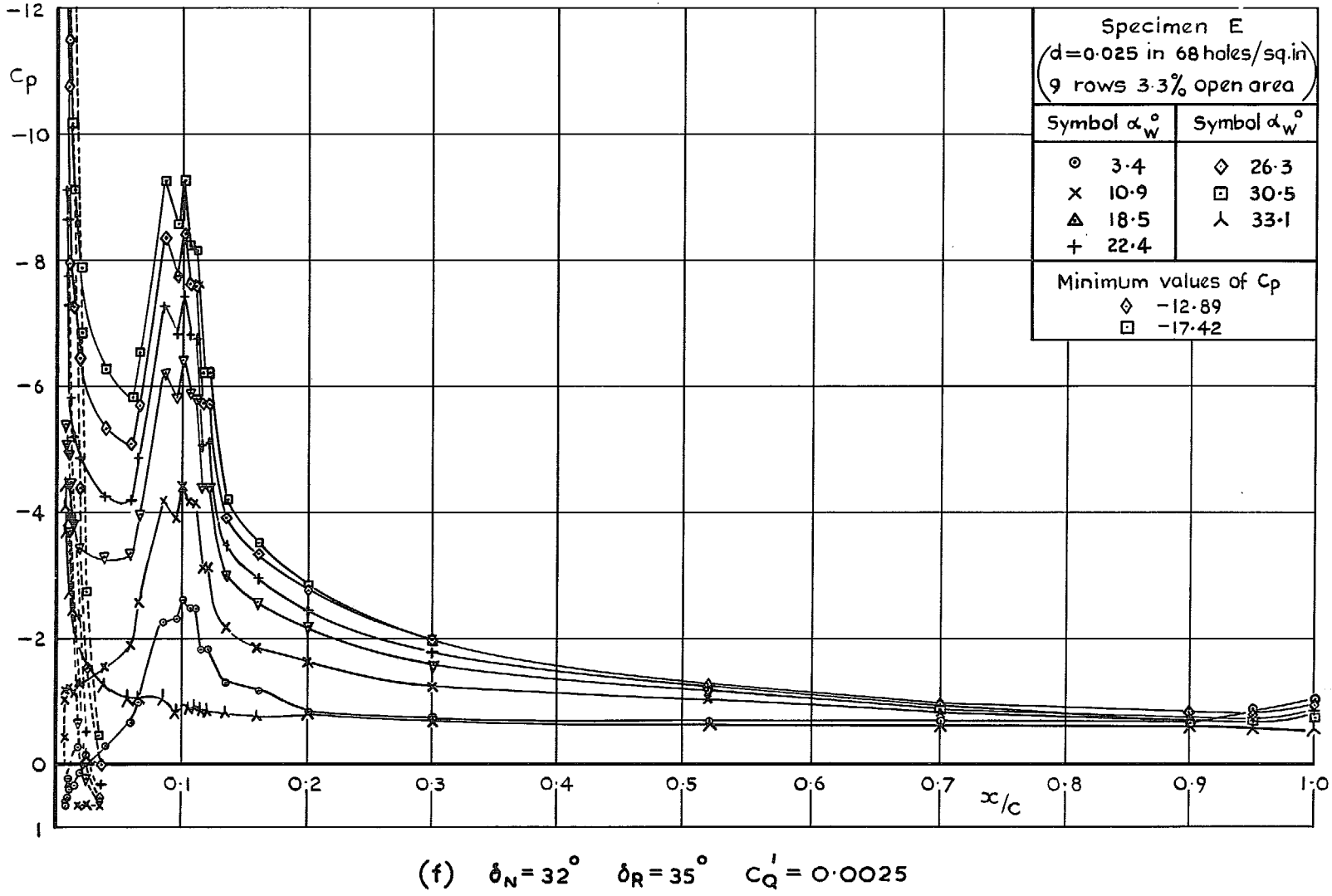


FIG. 16 (cont'd). The effect of distributed suction at knee of conventional L.E. flap on wing surface pressure distribution (0·656 $b/2$, starboard wing).

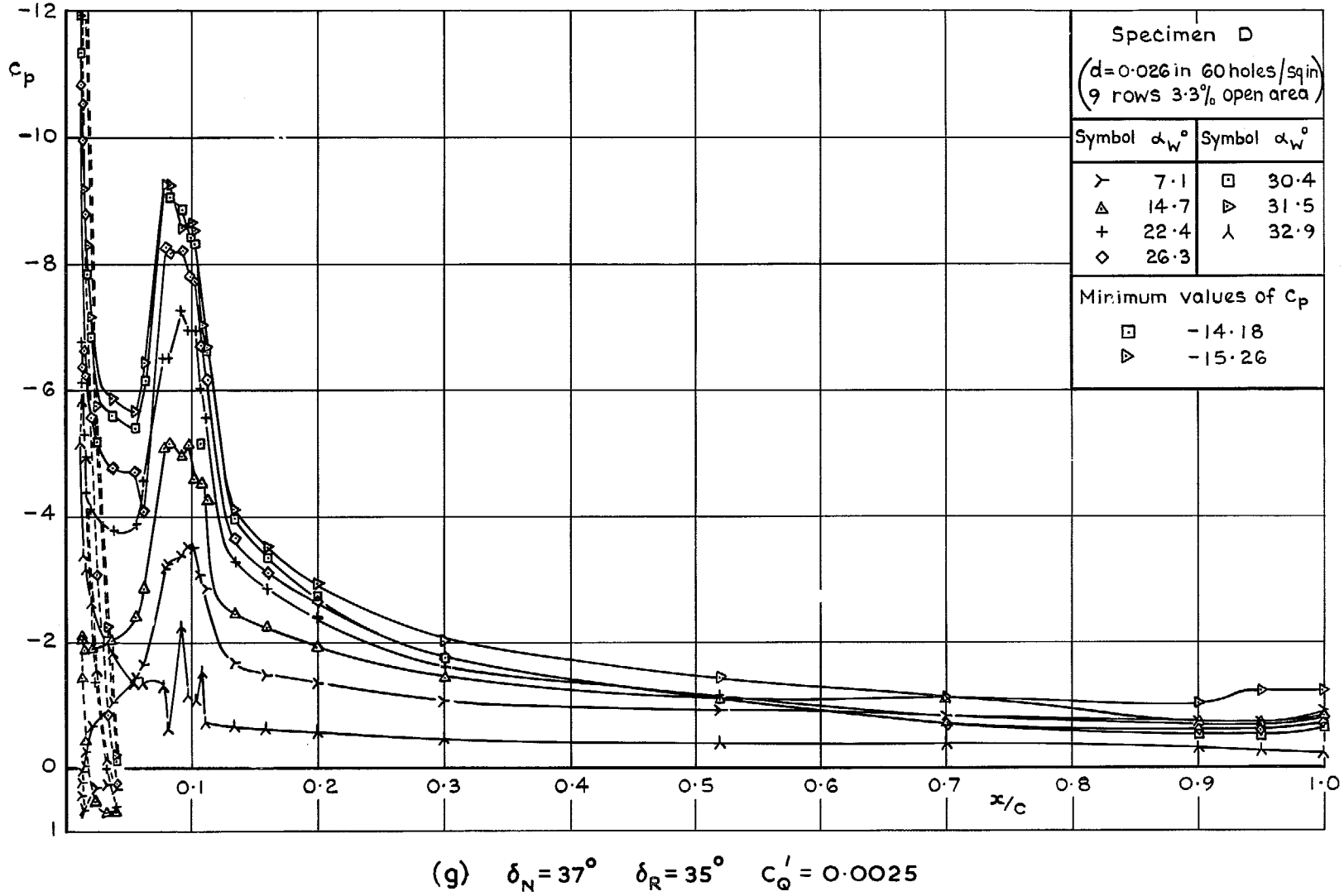


FIG. 16 (concld). The effect of distributed suction at knee of conventional L.E. flap on wing surface pressure distribution (0·656 $b/2$, starboard wing).

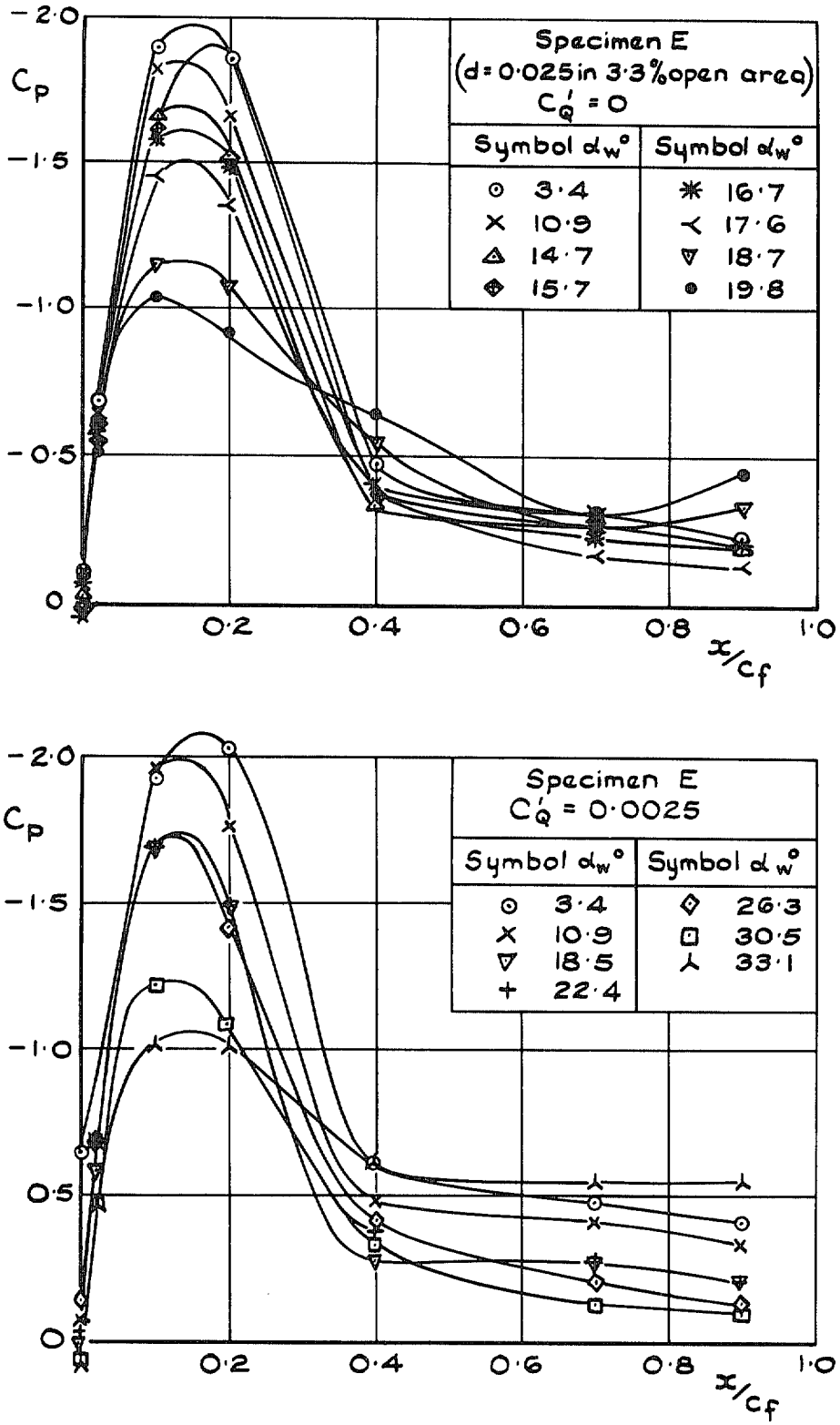


FIG. 17. The effect of distributed suction at knee of conventional L.E. flap on pressure distribution on T.E. Fowler flap.
0·652 $b/2$ starboard wing $\delta_N = 32°$ $\delta_R = 35°$.

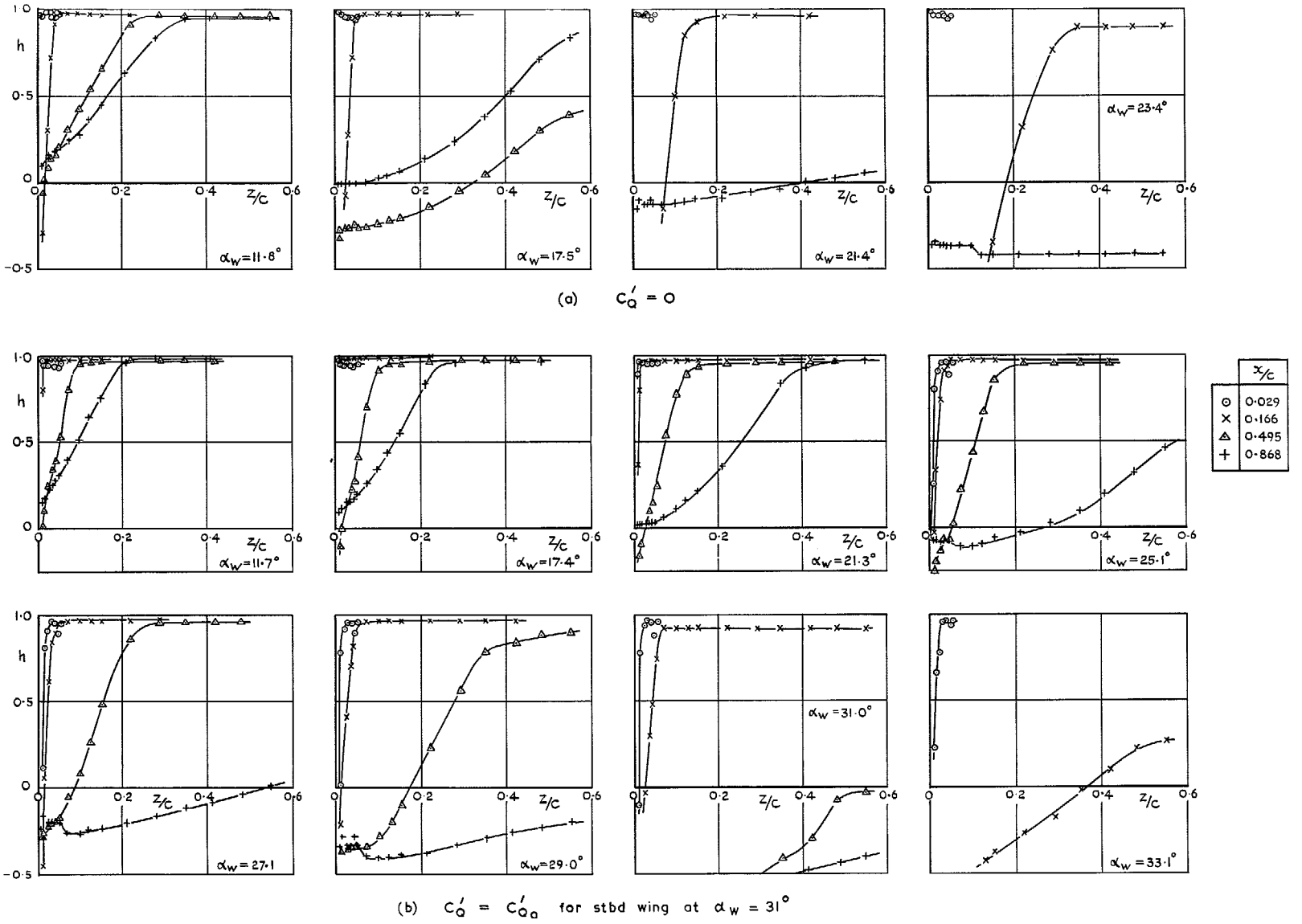


FIG. 18. The effect of distributed suction at knee of conventional L.E. flap on boundary layer profiles, starboard wing, $y = 0{\cdot}656\ b/2$ $\delta_\lambda = 32$ $\delta_R = 0$
Specimen E ($d$ = 0·025 in, 3·3 per cent open area).

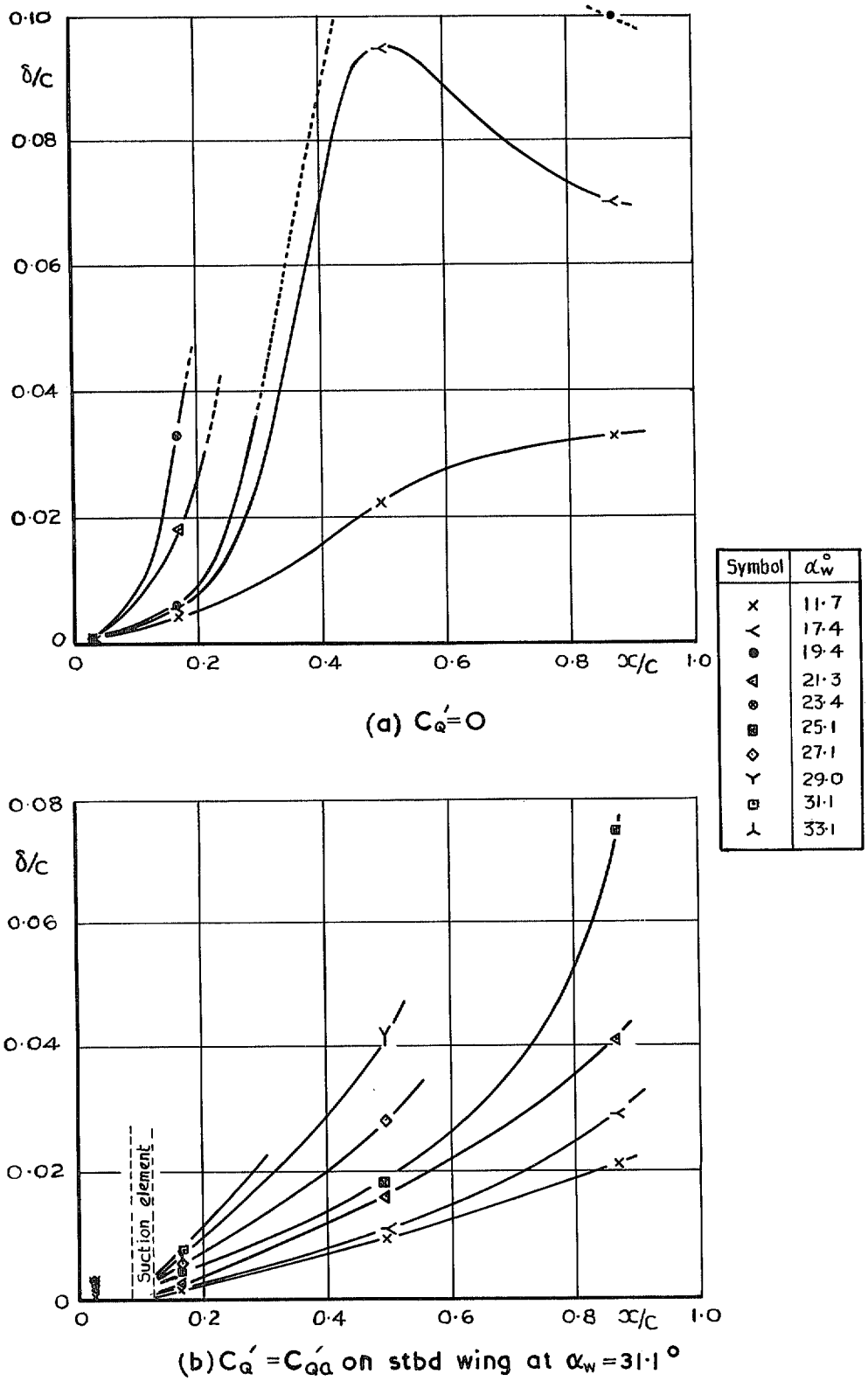


FIG. 19 a & b. The effect of distributed suction at knee of conventional L.E. flap on boundary layer thickness $\delta_N = 32°$ $\delta_R = 0°$ specimen E ($d = 0{\cdot}025$ in, 3·3 per cent open area).

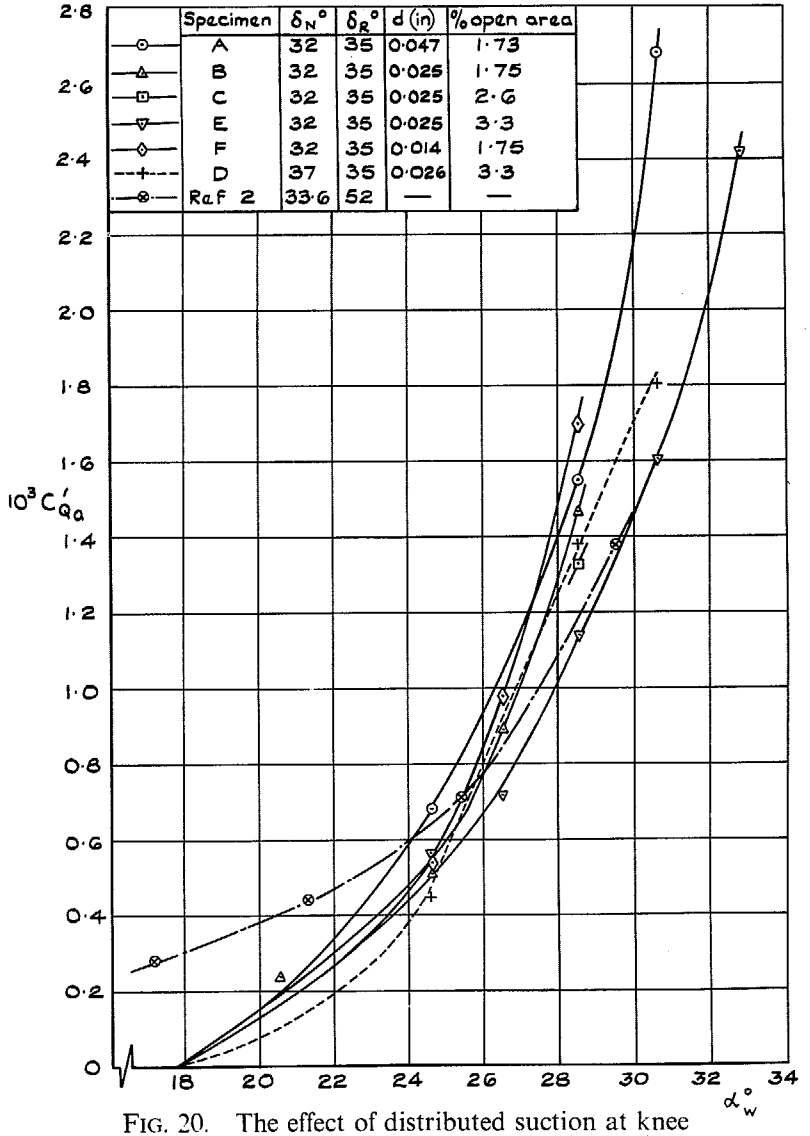


FIG. 20. The effect of distributed suction at knee of conventional L.E. flap on $C'_{Qa}$ *vs* $\alpha_w$ for various suction arrangements.

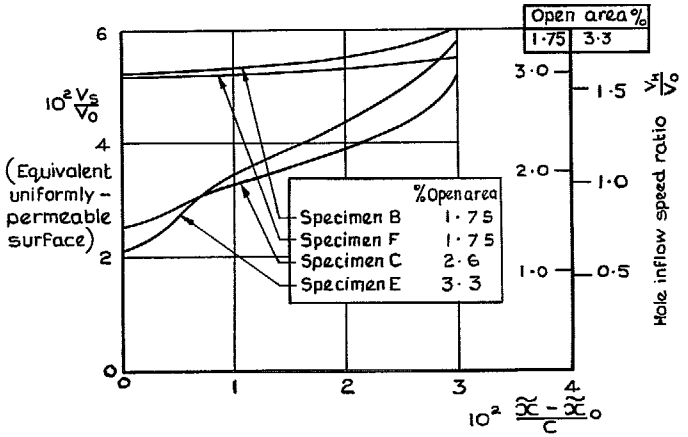


FIG. 21. Typical effect of open area ratio on chordwise inflow distribution at $C'_{Qa}$ with distributed suction at knee of conventional L.E. flap. $\delta_N = 32°$, $\delta_R = 35°$, $\alpha_W = 28°$.

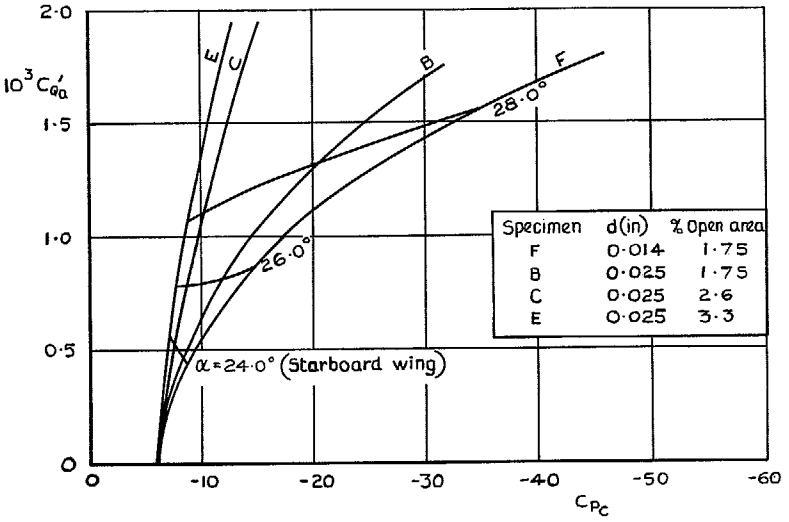


FIG. 22. The effect of open area ratio on $C'_Q$ *vs* $C_{p_c}$ with distributed suction at knee of conventional L.E. flap. $\delta_N = 32°$, $\delta_R = 35°$.

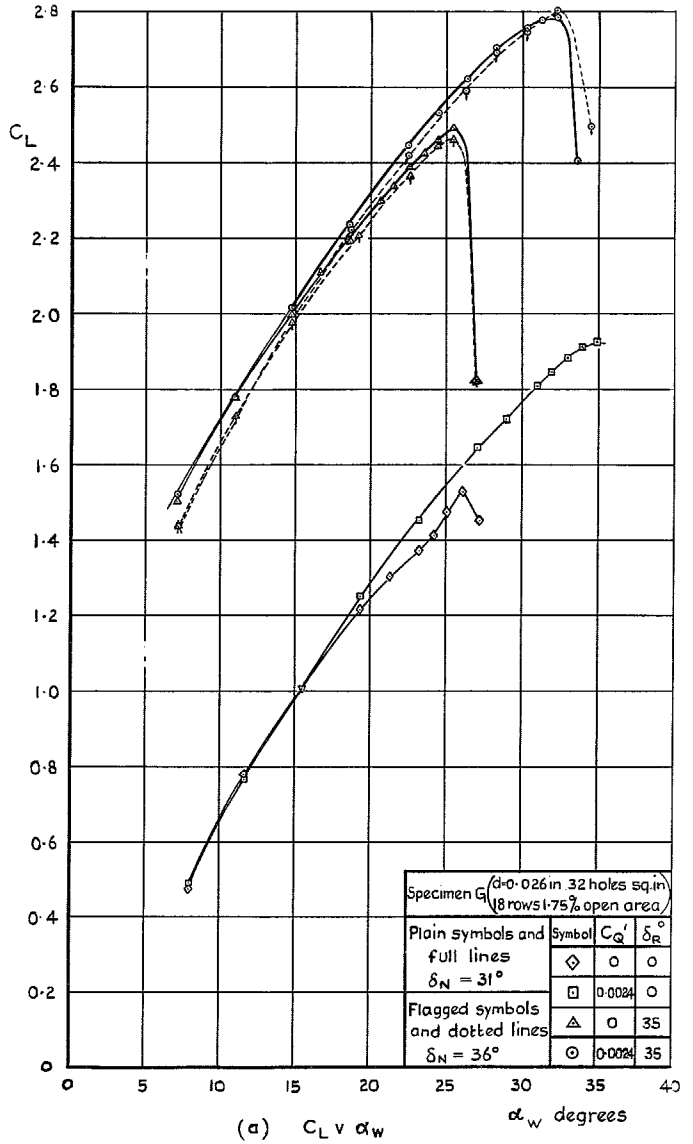


(a) $C_L$ v $\alpha_w$

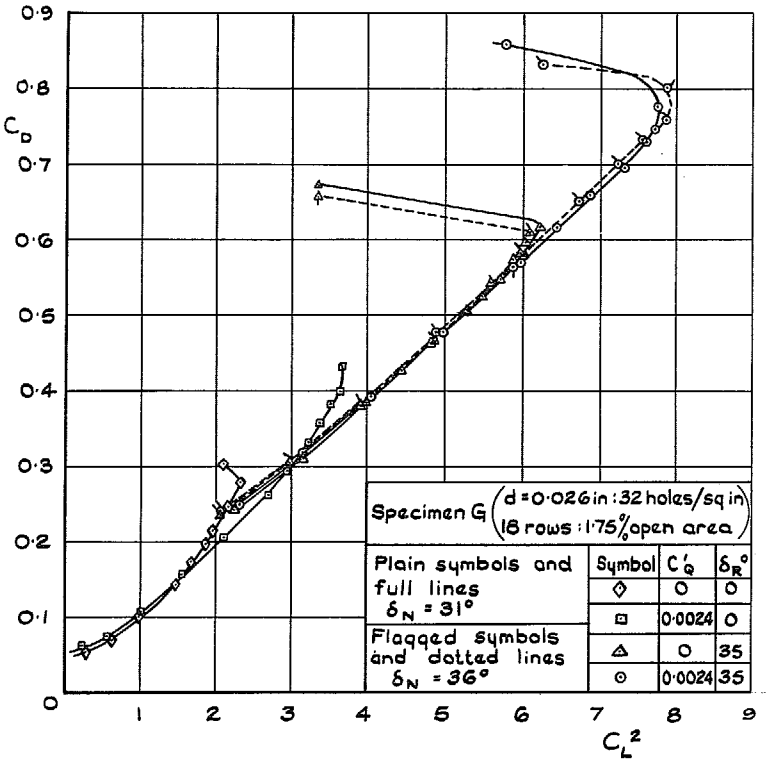


(b) $C_D$ v $C_L^2$

FIG. 23. The effect of distributed suction at knee of extending-area L.E. flap on force and moment characteristics.

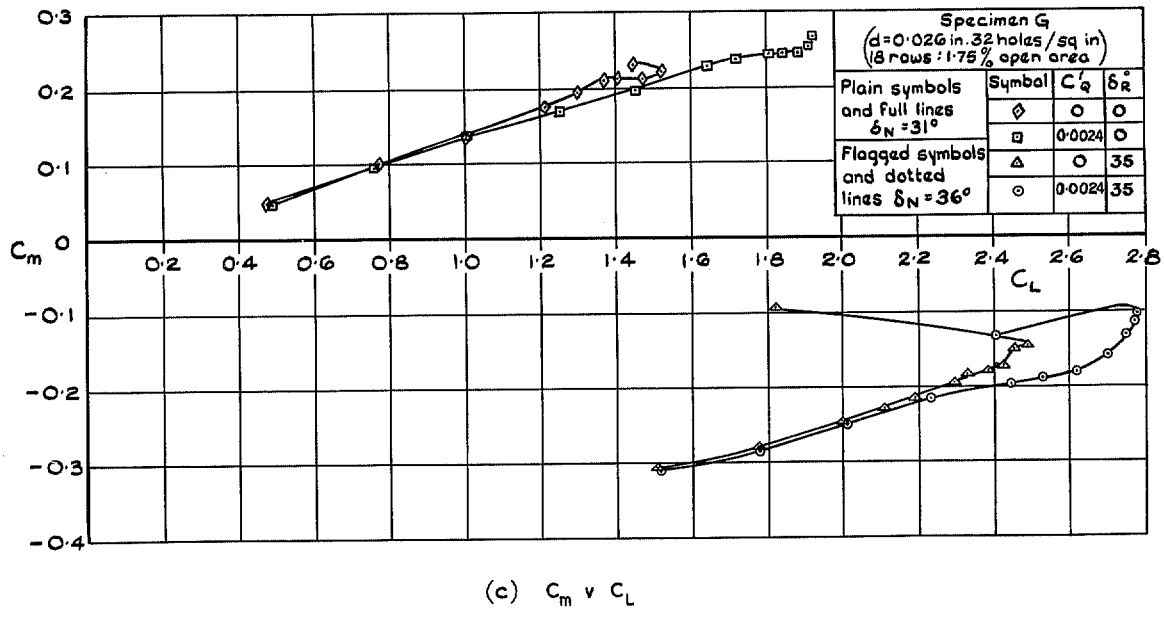


(c) $C_m$ v $C_L$

FIG. 23 (cont'd). The effect of distributed suction at knee of extending-area L.E. flap on force and moment characteristics.

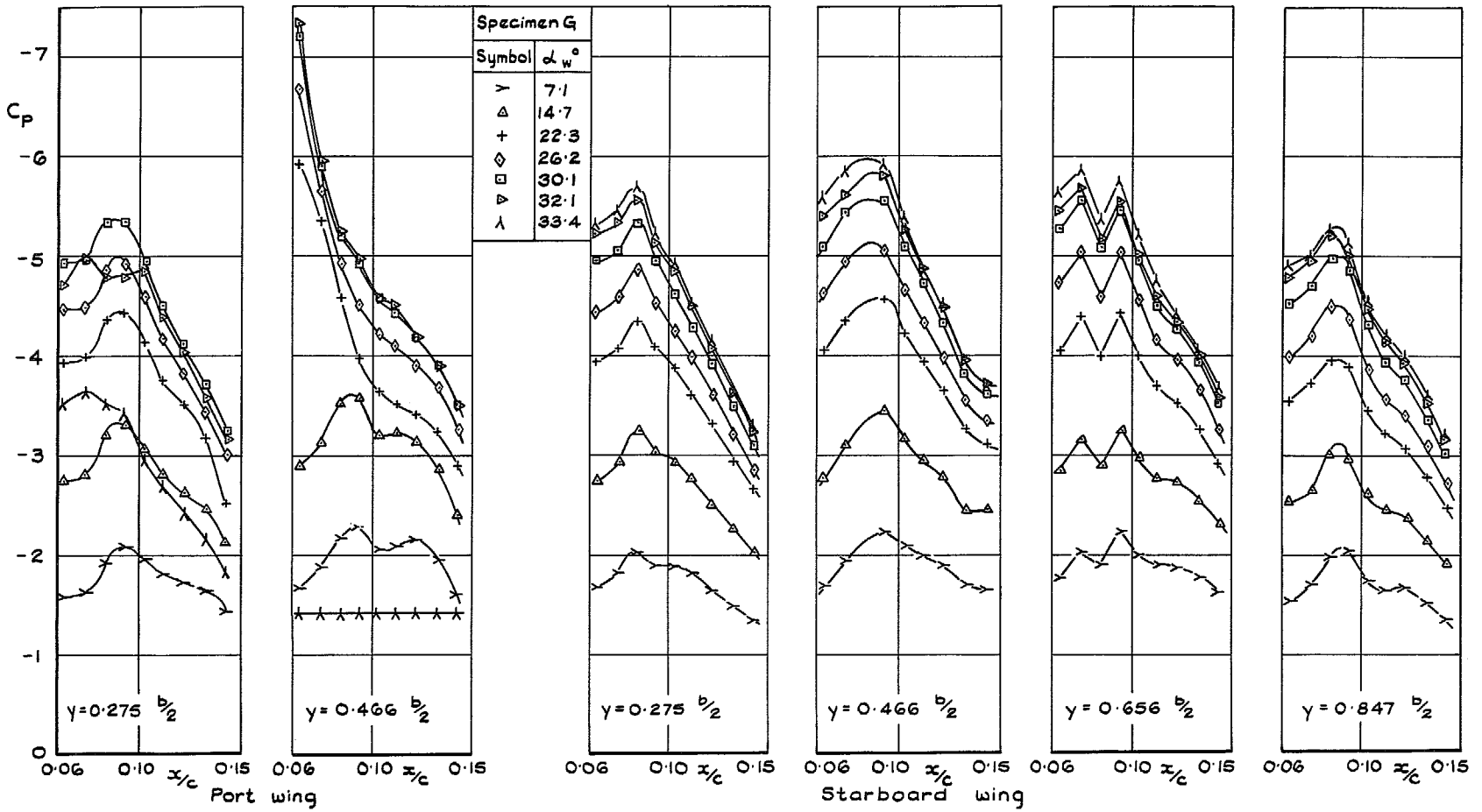


FIG. 24. Spanwise variations of surface pressure at knee of extending area L.E. flap with distributed suction $\delta_N = 31$, $\delta_R = 35$, $C'_Q = 0{\cdot}0024$

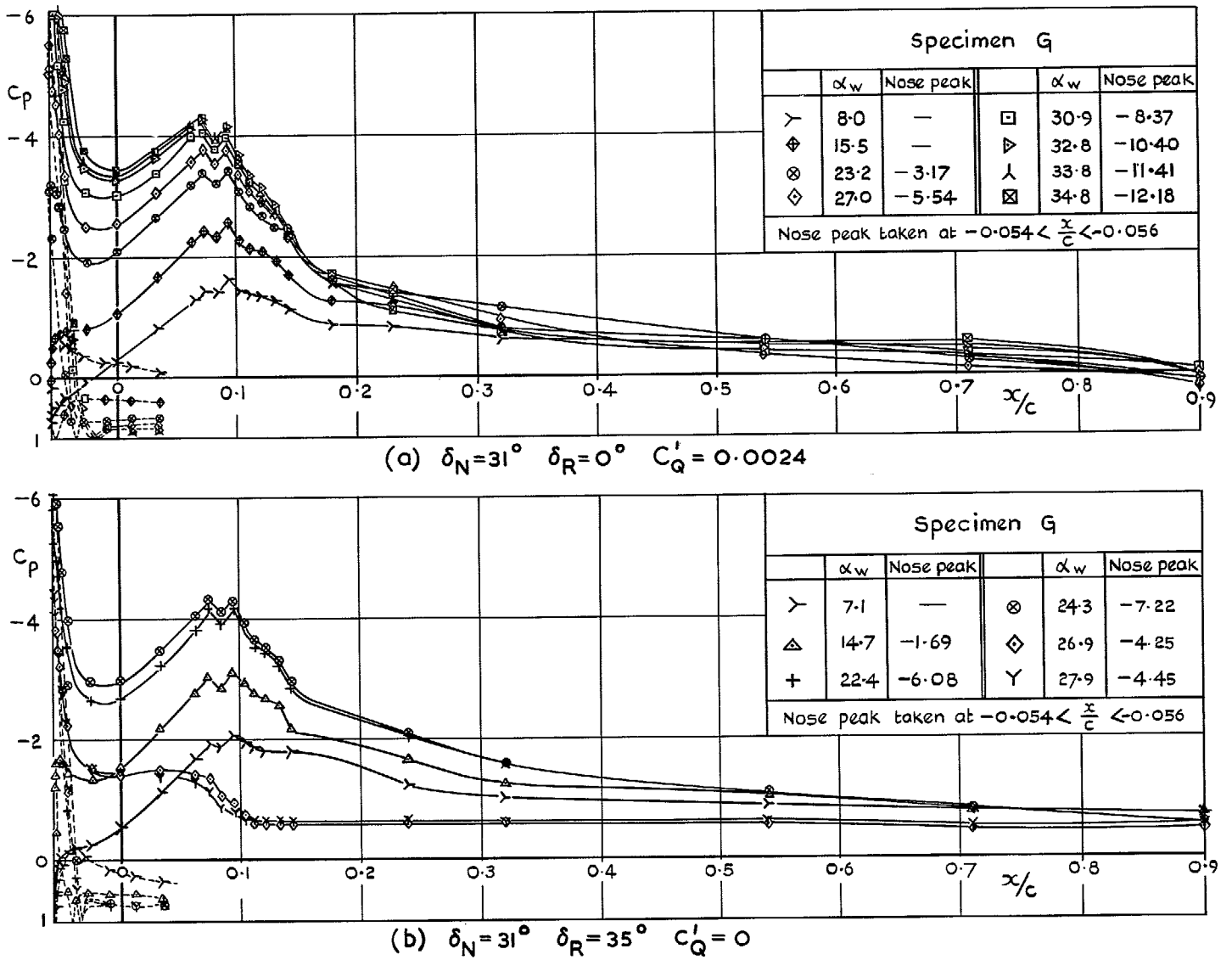


FIG. 25. The effect of distributed suction at knee of extending area L.E. flap on wing surface pressure distribution (0·656 *b*/2, starboard wing).

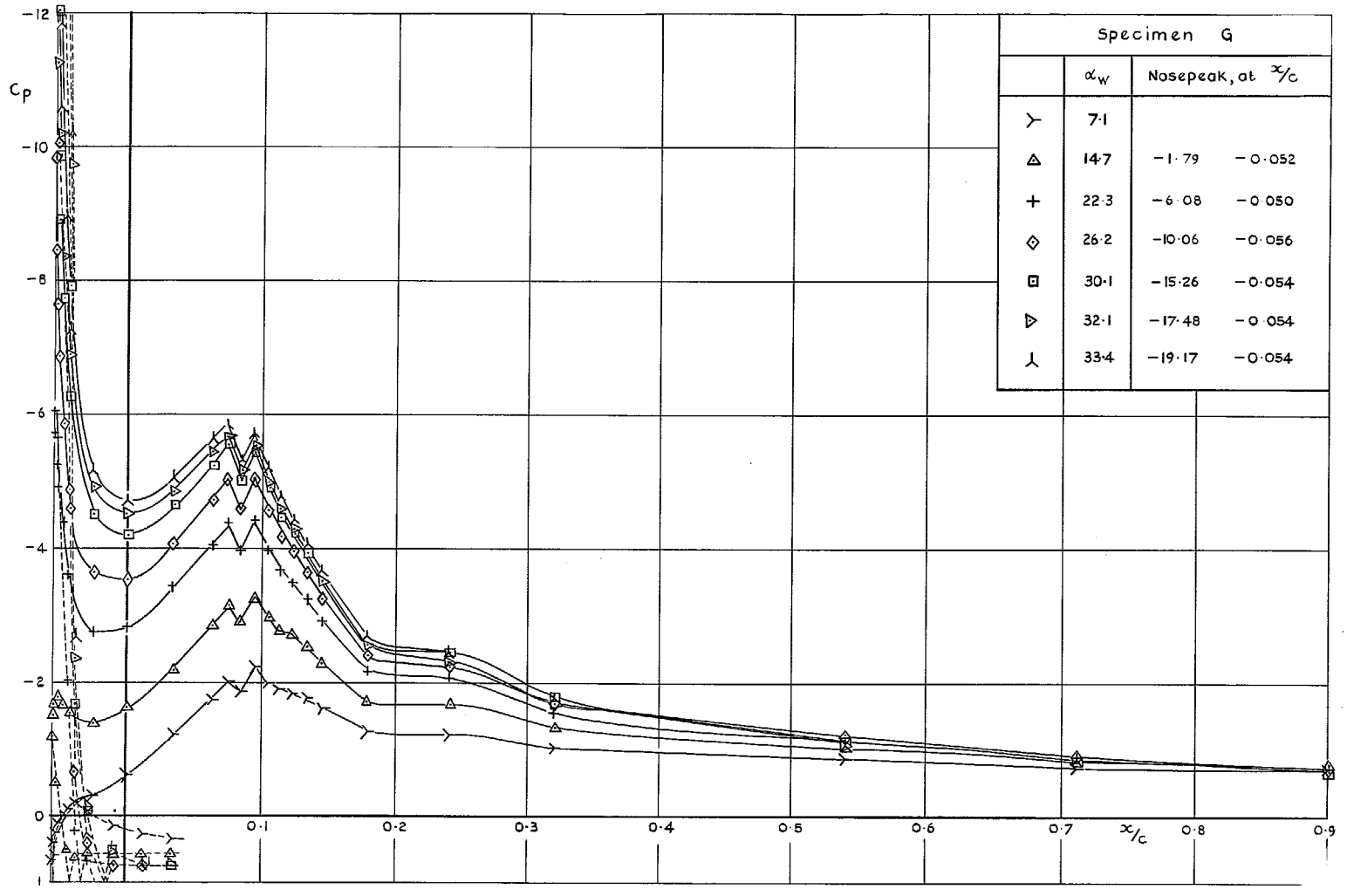


(c) $\delta_N = 31°$ $\delta_R = 35°$ $C_Q' = 0{\cdot}0024$

FIG. 25 (cont'd). The effect of distributed suction at knee of extending area L.E. flap on wing surface pressure distribution (0·656 $b/2$, starboard wing).

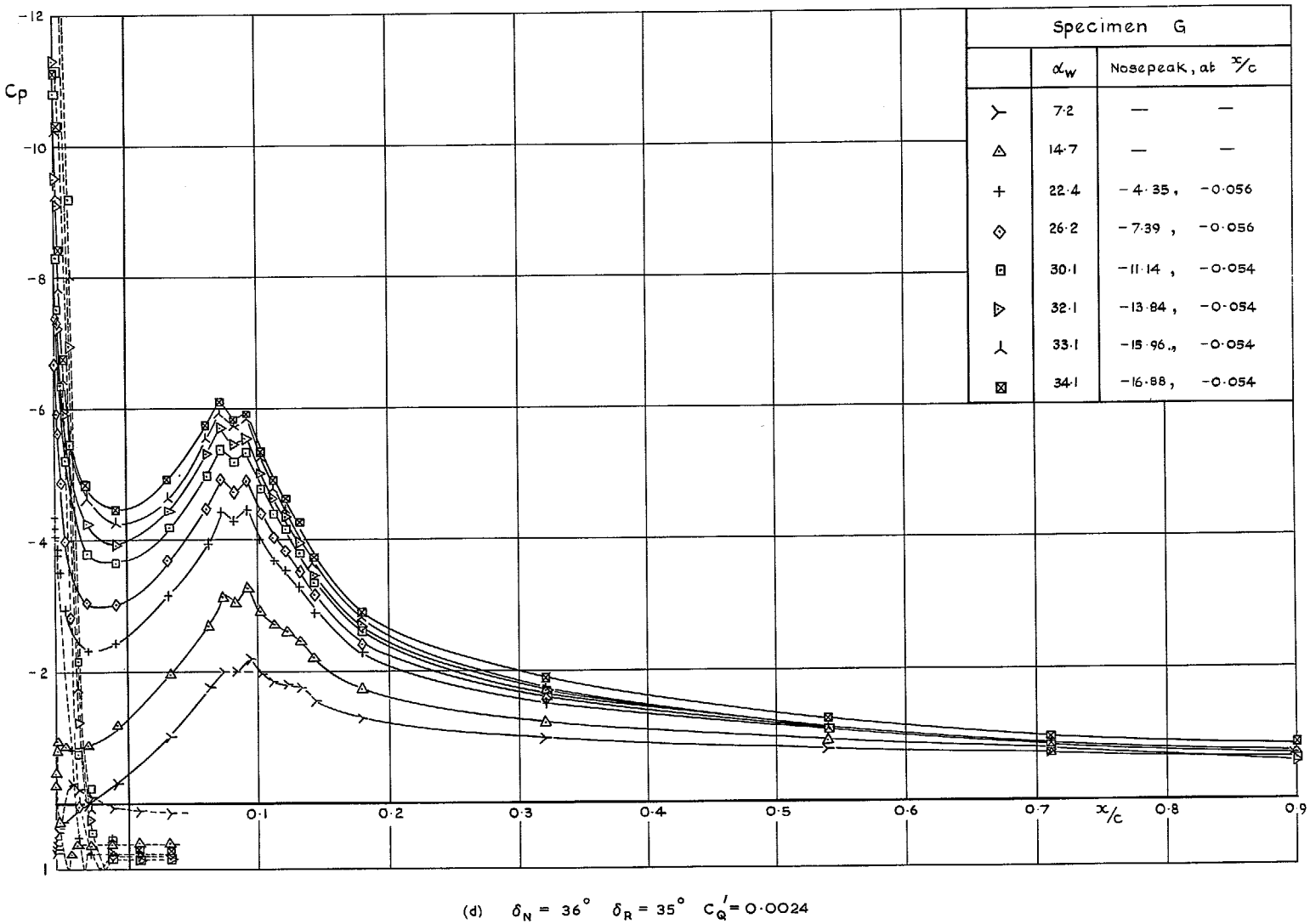


FIG. 25 (concld). The effect of distributed suction at knee of extending area L.E. flap on wing surface pressure distribution (0·656 $b/2$, starboard wing).

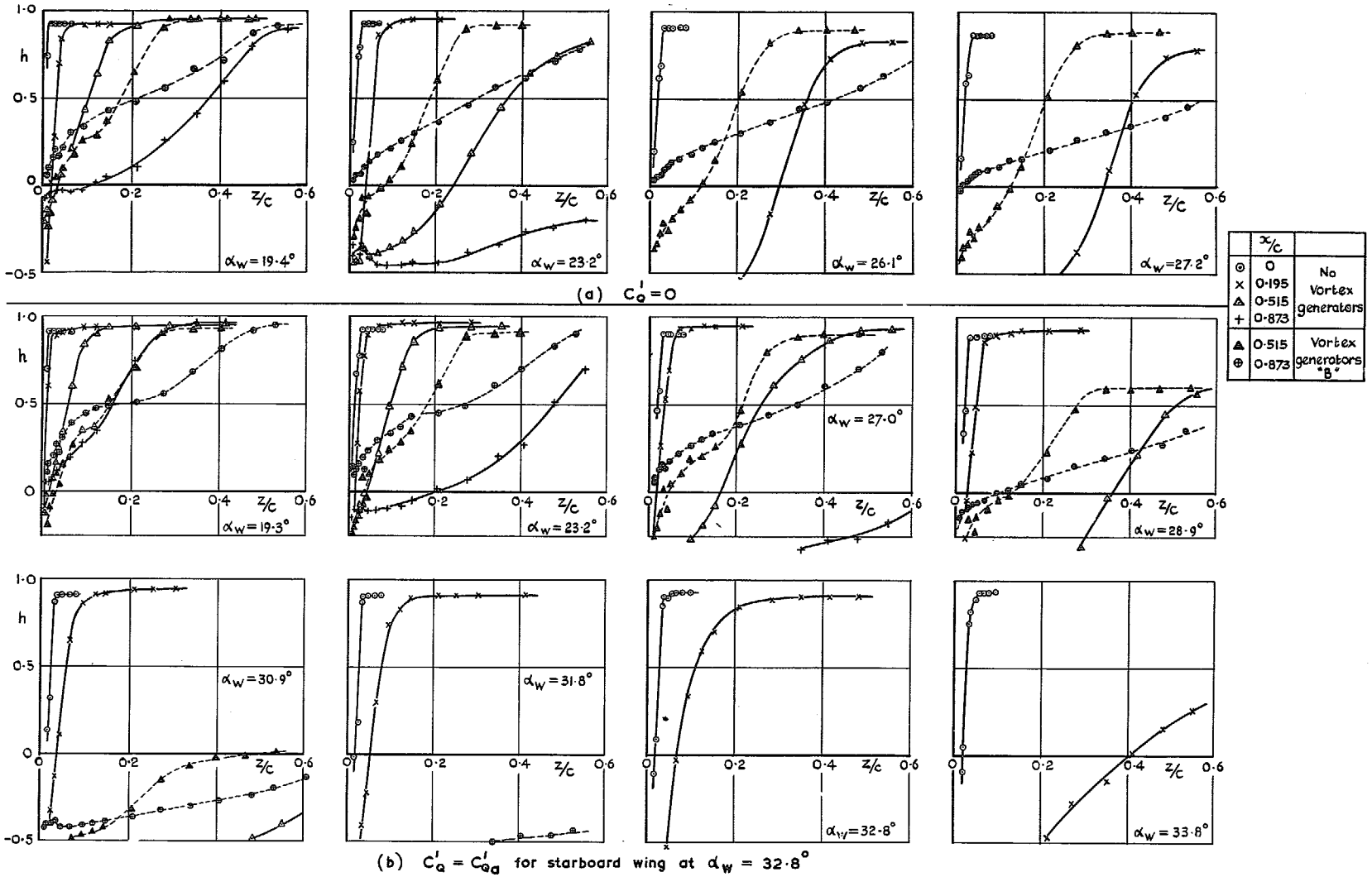


FIG. 26. The effect of distributed suction at knee of extending area L.E. flap on boundary-layer profiles. Starboard wing, $y = 0{\cdot}656\ b/2$, $\delta_N = 31°$, $\delta_R = 0°$, specimen $G$ ($d = 0{\cdot}026$ in 1·75 per cent open area).

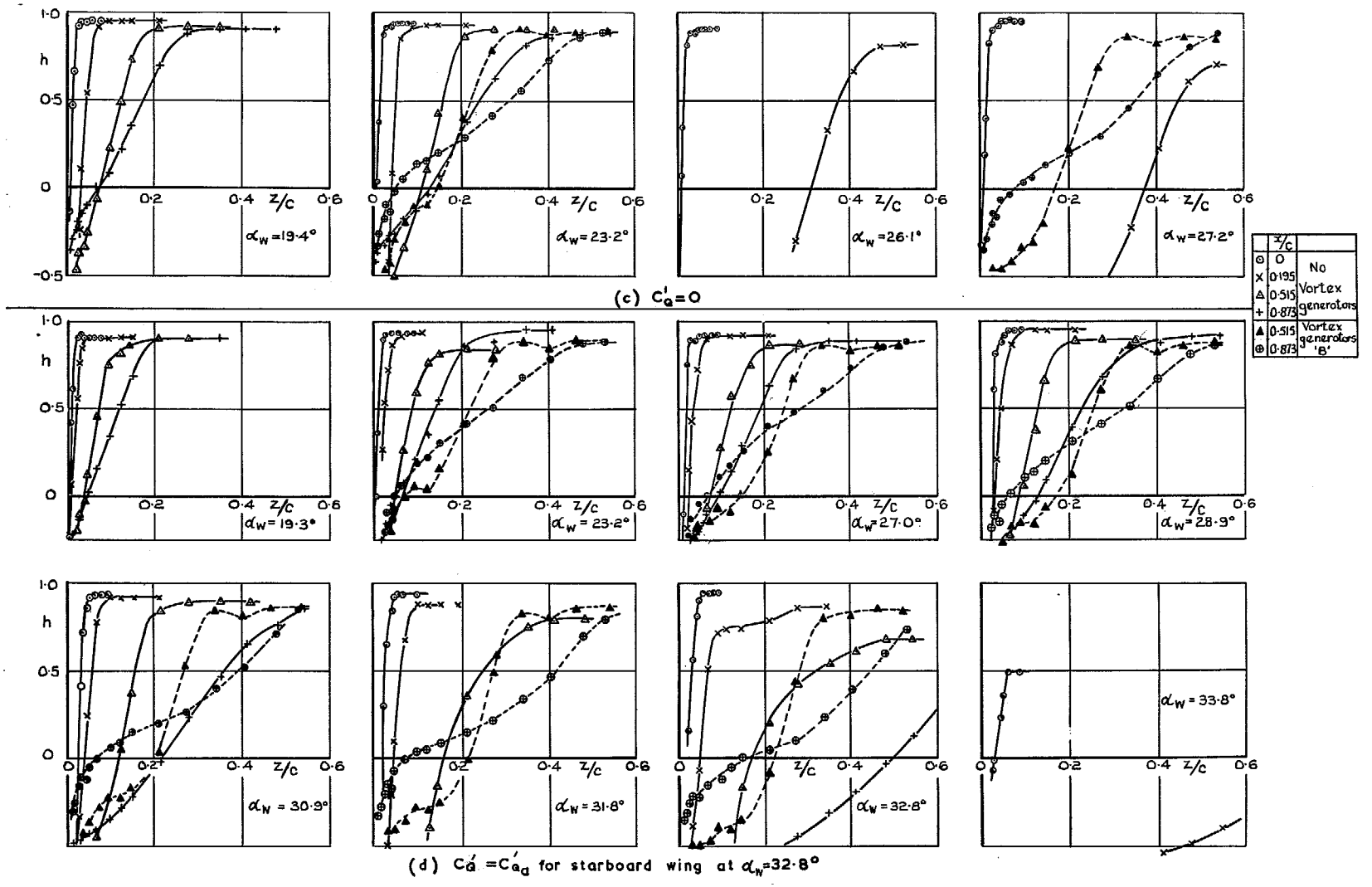


FIG. 26. The effect of distributed suction at knee of extending area L.E. flap on boundary-layer profiles profiles. Starboard wing $y = 0{\cdot}656\ b/2$, $\delta_N = 31°$, $\delta_R = 35°$, specimen G ($d = 0{\cdot}026$ in 1·75 per cent open area).

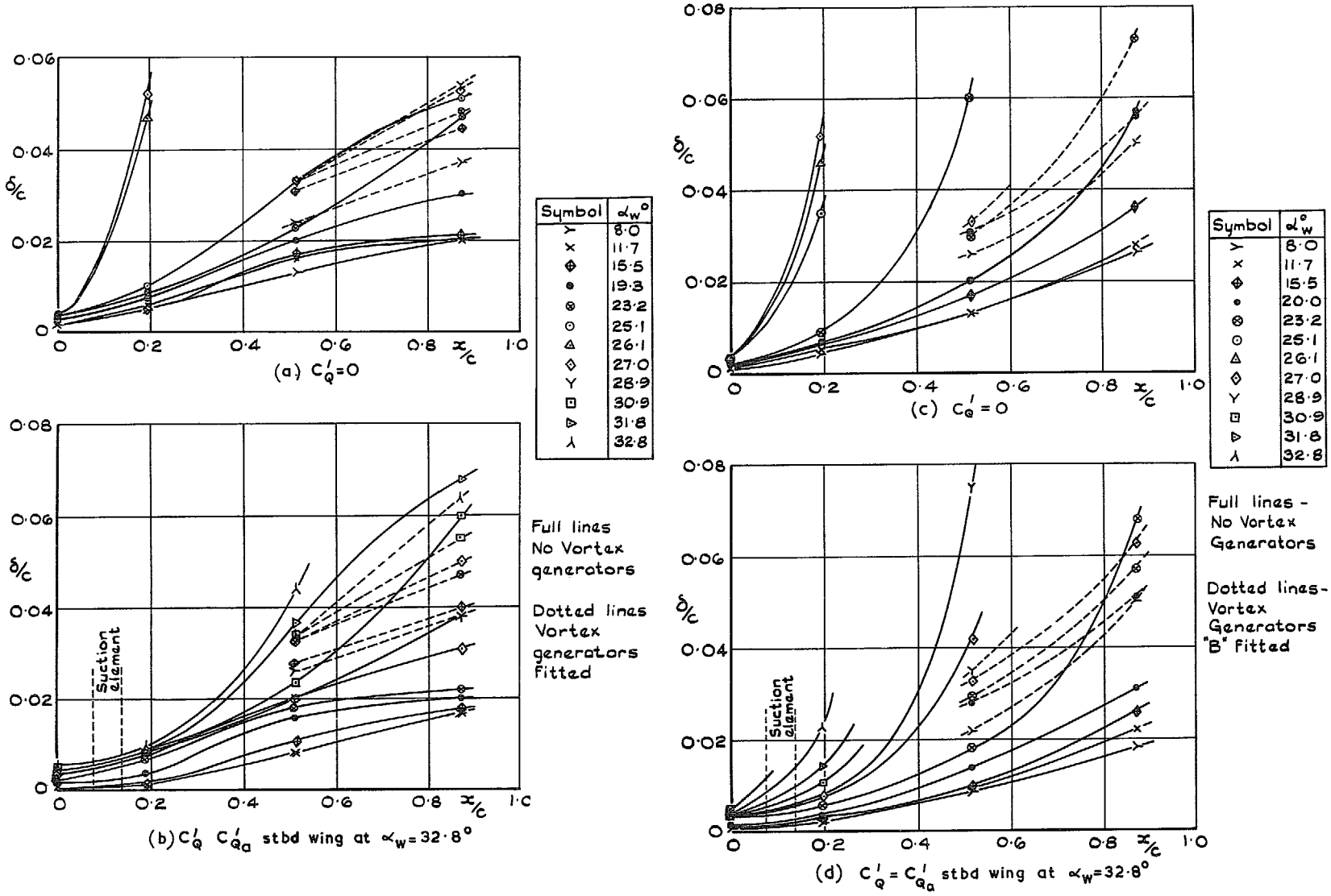


FIG. 27. The effect of distributed suction at knee of extending-area L.E. flap on boundary-layer thickness $\delta_N = 31°$ $\delta_R = 35°$ specimen G ($d = 0{\cdot}026$ in, 1·75 per cent open area).

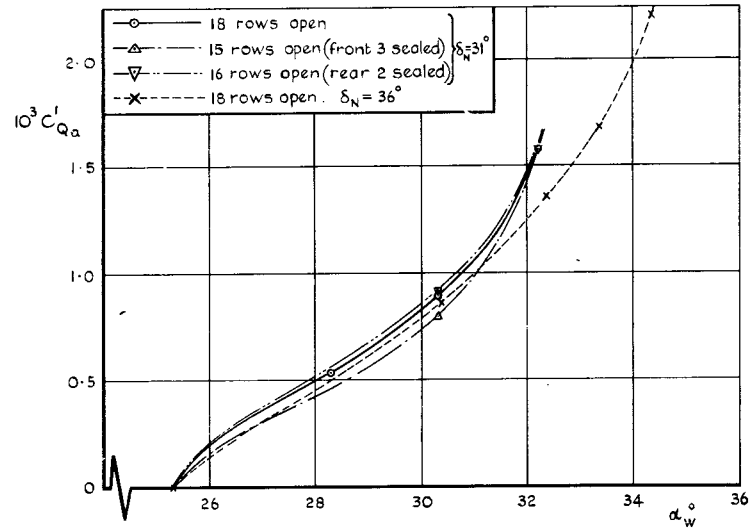


FIG. 28. The effect of distributed suction at knee of extending-area L.E. flap on $C'_{Q_a}$ *vs* $\alpha_W$, for various suction surface arrangements.
Specimen G ($d$ = 0·026 in, 1·75 per cent open area). $\delta_R$ = 35°.

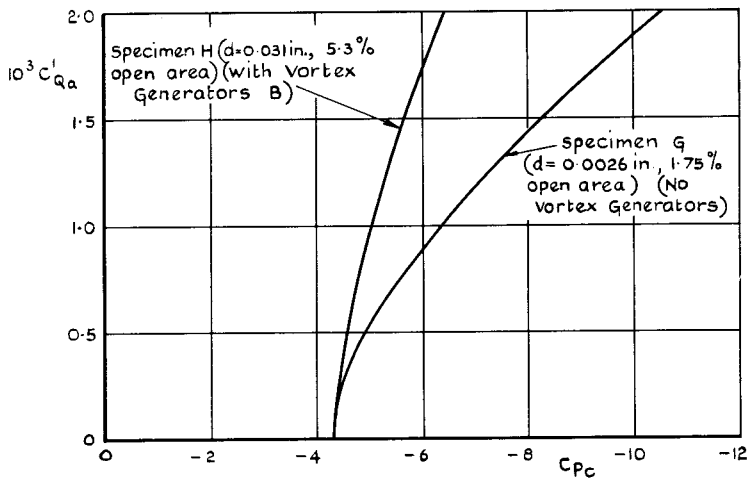


FIG. 29. The effect of distributed suction at knee of extending-area L.E. flap on $C'_{Q_a}$ *vs* $C_{p_{\tilde{c}}}$, for various suction surface arrangements. $\delta_R$ = 35°.

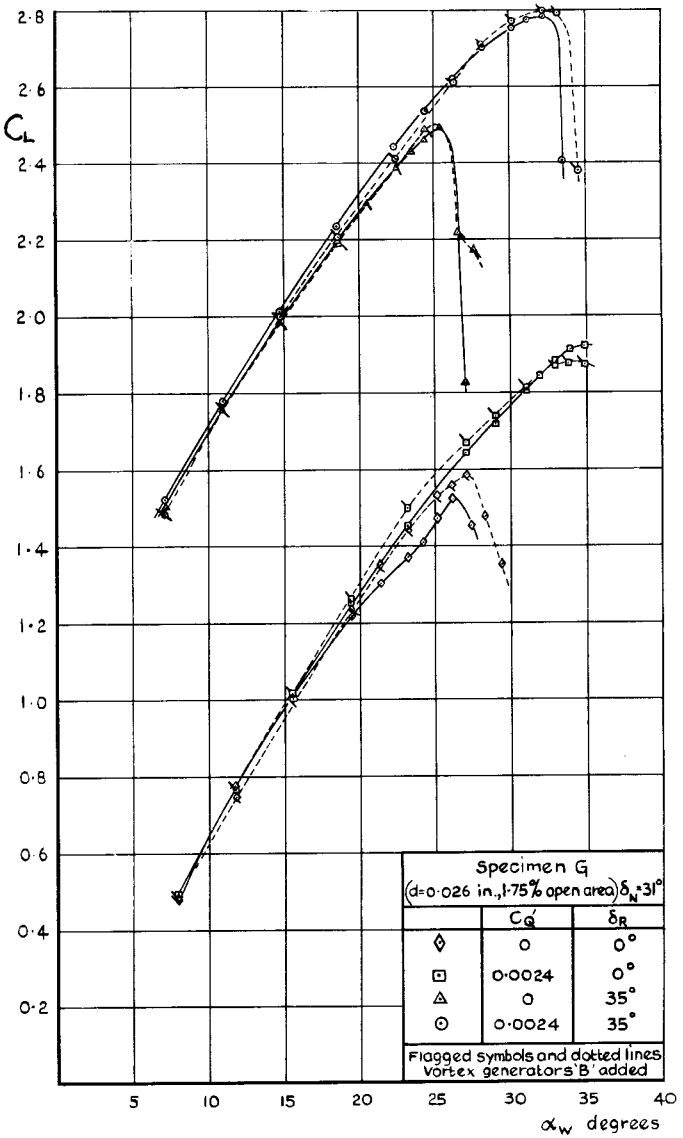


FIG. 30. The effect of mid-chord vortex generators on $c_L$ *vs* $\alpha_W$, with distributed suction at knee of extending-area L.E. flap.

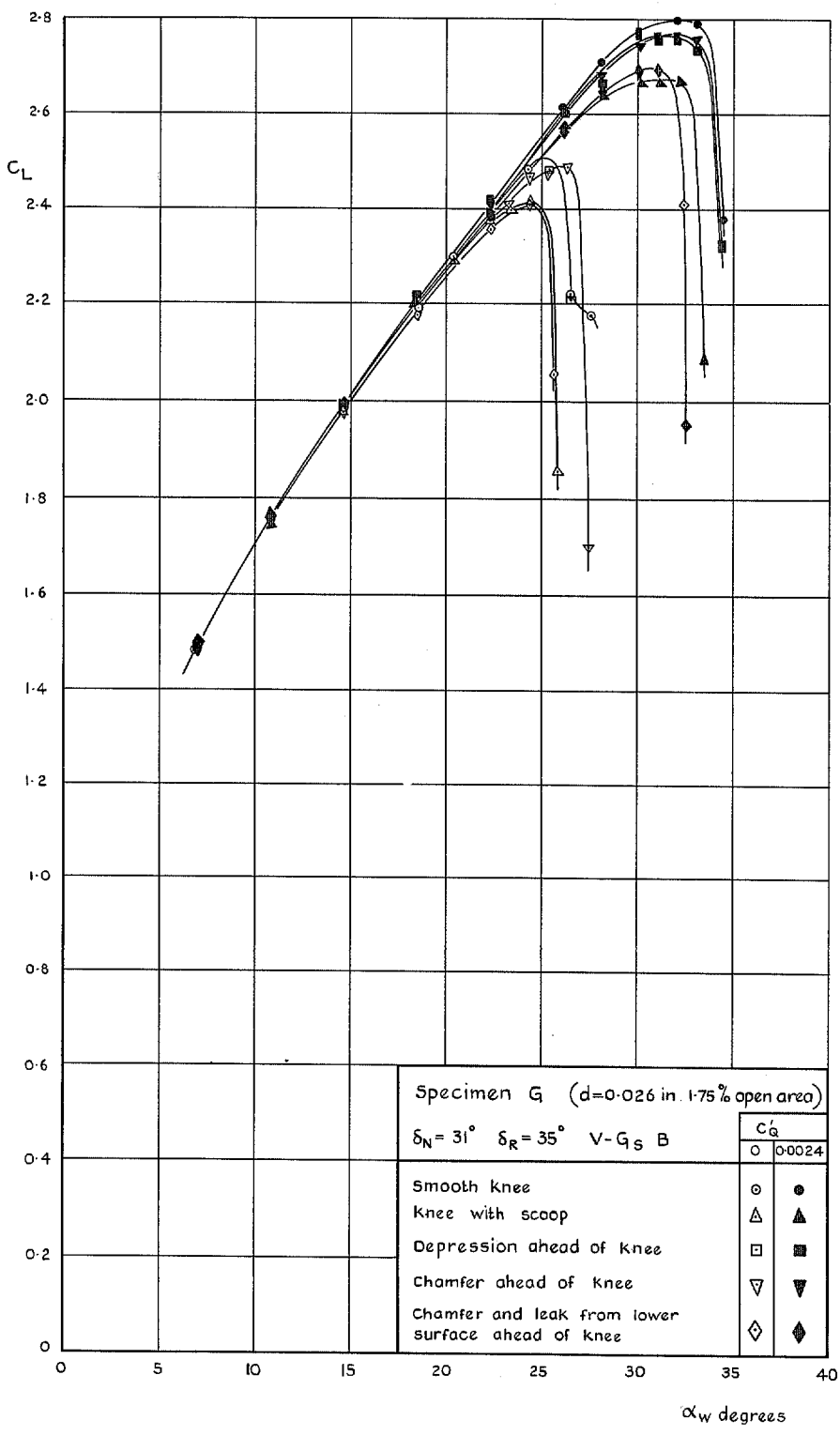


FIG. 31. The effect of various surface imperfections on $C_L$ *vs* $\alpha_w$, with distributed suction at knee of extending-area L.E. flap.

Printed in Wales for Her Majesty's Stationery Office by Allens Printers (Wales) Limited.
Dd. 501372 K5.



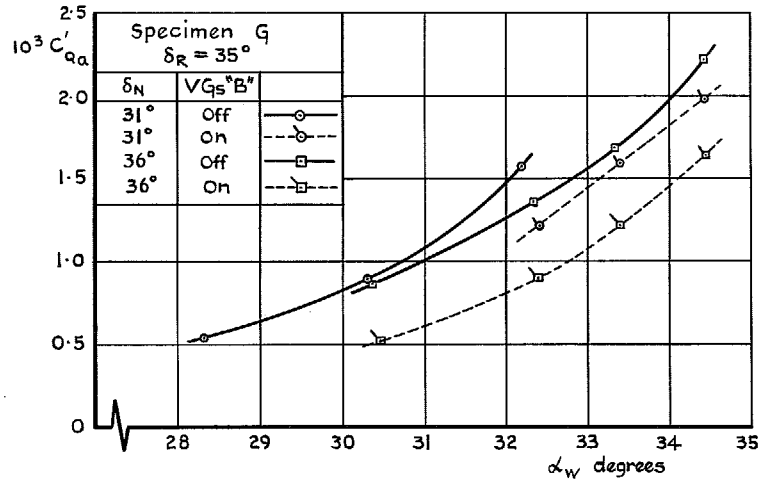


FIG. 32. The effect of mid-chord vortex generators on $C'_{Q_a}$ *vs* $\alpha_W$, extended-area L.E. flap.

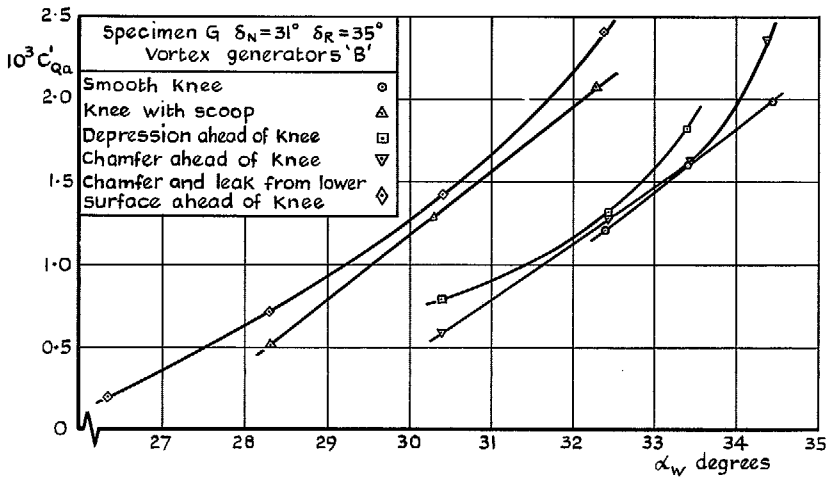


FIG. 33. The effect of various surface imperfections on $C'_{Q_a}$ *vs* $\alpha_W$, extended-area L.E. flap.

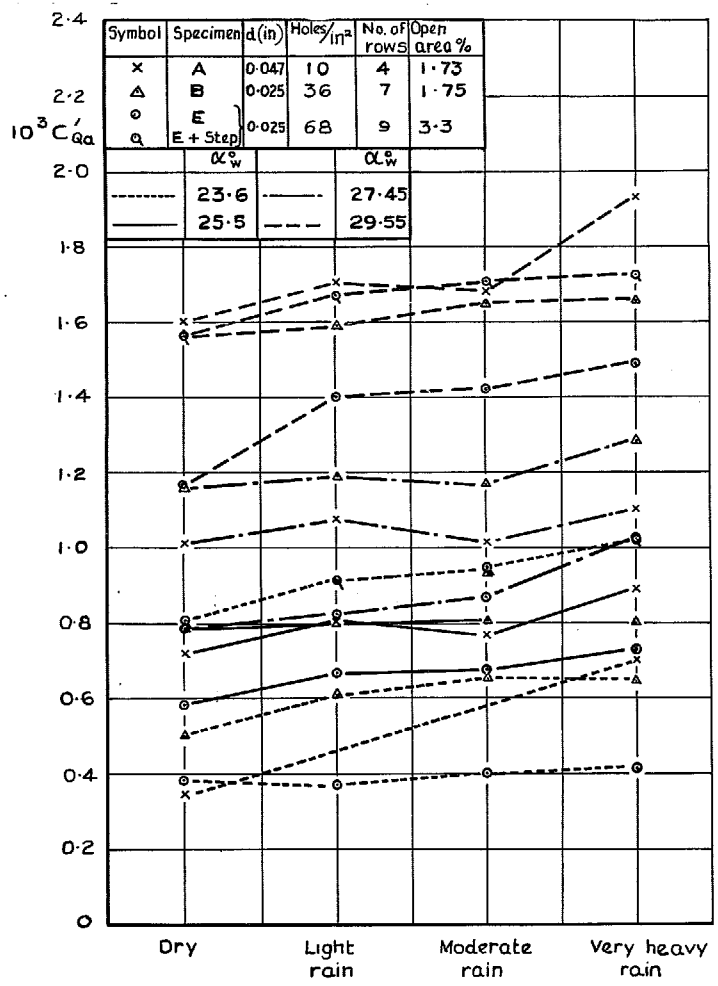


FIG. 34. The effect of rain on $C'_{Q_a}$, with distributed suction at knee of conventional L.E. flap. $\delta_N = 32°$, $\delta_R = 35°$.

Published by
HER MAJESTY'S STATIONERY OFFICE

To be purchased from
49 High Holborn, London WC1 6HB
13a Castle Street, Edinburgh EH2 3AR
109 St Mary Street, Cardiff CF1 1JW
Brazennose Street, Manchester M60 8AS
50 Fairfax Street, Bristol BS1 3DE
258 Broad Street, Birmingham 1
7 Linenhall Street, Belfast BT2 8AY
or through any bookseller

R. & M. No. 3640
SBN 11 470340 X